1-1-2007

Study on the shear behavior of prestressed concrete hollow core slabs by nonlinear finite element modelling.

Xuefei Wang
University of Windsor

Study on the Shear Behavior of Prestressed Concrete Hollow Core Slabs by Nonlinear Finite Element Modelling

By

Xuefei Wang

A Thesis

Submitted to the Faculty of Graduate Studies

Through Civil & Environmental Engineering

in Partial Fulfillment of the Requirements for

the Degree of Master of Applied Science at the

University of Windsor

Windsor, Ontario, Canada

2007

Your file Votre référence
ISBN: 978-0-494-35048-5
Our file Notre référence
ISBN: 978-0-494-35048-5

ABSTRACT

Three-dimensional finite element models of prestressed concrete hollow core slabs and I-shaped concrete beams are developed to study their shear behavior. Nonlinear finite element analysis is performed using the ANSYS 2003 software. SOLID65, LINK8, and SOLID45 elements are selected to represent the behavior of concrete, discrete reinforcing steel bars and steel plate, respectively. By applying transverse concentrated load, the load-deflection response of hollow core slabs and I-shaped concrete beams derived from the numerical models are presented. These results are then compared with the data obtained from physical tests to verify the validity and accuracy of the numerical models. Comparisons have been made among the shear strength of hollow core slabs and I-shaped beams obtained from the numerical models, physical tests and ACI 318 code. It has been found that in most cases, the results from the numerical simulation agree well with those from the physical tests. Also, results show that while the ACI 318 code can well predict the shear strength of I-shaped concrete beams, its prediction on the shear strength of prestressed concrete hollow core slabs is much more conservative when compared with those obtained from the numerical simulation and the physical tests.

ACKNOWLEDGEMENT

I would like to express my deep and sincere gratitude to my supervisor, Professor Shaohong Cheng, Department of Civil & Environmental Engineering and Department of Mechanical, Automotive and Materials Engineering, University of Windsor. Her wide knowledge and her logical way of thinking have been of great value for me. Her understanding, encouraging and personal guidance have provided a good basis for the present thesis.

I want to thank the Department of Civil & Environmental Engineering and The Prestressed group (PSI) for giving me opportunity and specimen to commence this thesis in the first instance, to do the necessary research work and to use departmental data.

Especially, I would like to give my special thanks to my wife Chunning Li whose patient love enabled me to complete this work.

TABLE OF CONTENTS

LIST OF FIGURES

LIST OF TABLES

LIST OF SYMBOLS

V_{ci}	nominal shear strength of concrete in a shear-flexure failure mode;
V_{cw}	nominal shear strength of concrete in a web shear failure mode;
$f_c^{'}$	specified compressive strength of concrete;
f_{pc}	compressive stress in concrete at the centroid of the section due to effective prestress for non –composite sections;
b_w	net web width of hollow core slab;
d	distance from extreme compression fiber to the centroid of tension reinforcement;
V_p	vertical component of effective prestressing force;
V_d	shear due to unfactored load;
M_{cr}	cracking moment;
M_{max}	maximum factored moment due to externally applied loads;
F	a function of the principal stress state ($\sigma_{xp}, \sigma_{yp}, \sigma_{zp}$);
$\sigma_{xp}, \sigma_{yp}, \sigma_{zp}$	principal stresses in the principal directions X, Y and Z;
S	failure surface (to be discussed) expressed in terms of principal stresses and five input parameters f_t, f_c , f_{cb} , f1 and f2;
f_t	ultimate uniaxial tensile strength;
f_c	uniaxial crushing strength;

f_{cb} ultimate biaxial compressive strength;

f_1 ultimate compressive strength for a state of biaxial compression superimposed on hydrostatic stress state;

f_2 ultimate compressive strength for a state of uniaxial compression superimposed on hydrostatic stress state.

CHAPTER 1 Literature Review

1.1 Introduction

A hollow core slab is a precast, prestressed concrete member with continuous voids provided to reduce its self-weight and fabrication cost. Though primarily used as floor or roof deck systems, hollow core slabs also have other applications such as wall panels and bridge deck units. Figure 1.1 shows the typical hollow core slab products used in roof and floor systems.

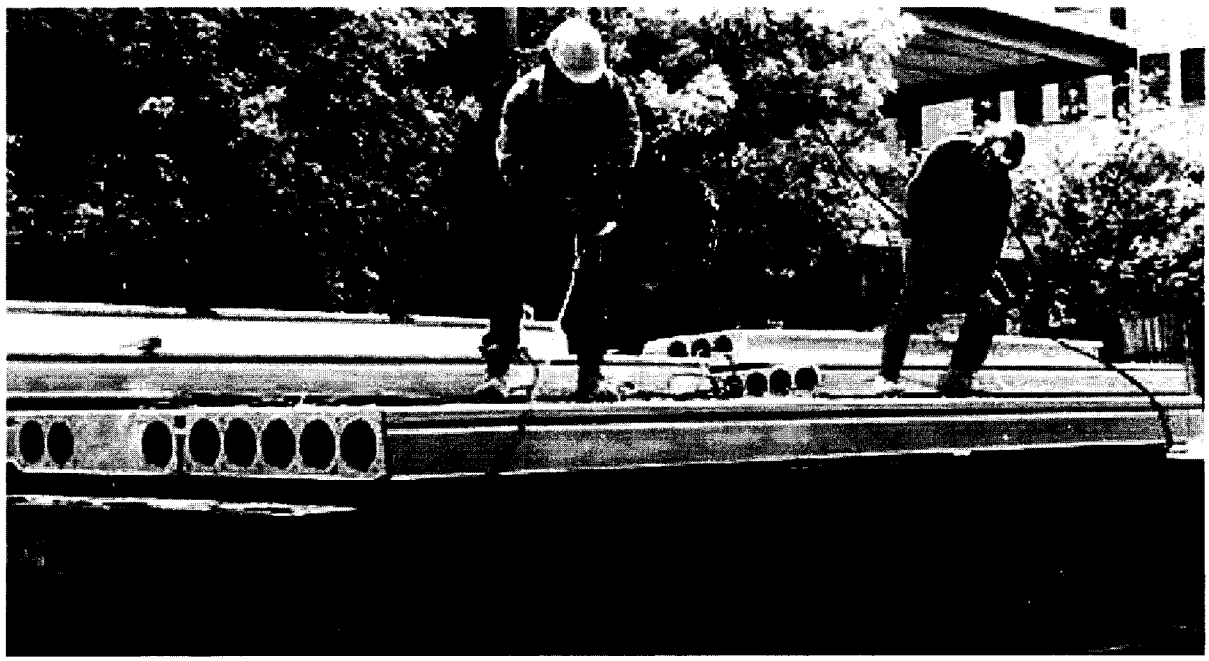

Figure 1.1: Hollow Core Slabs

The load bearing capacity of hollow core slabs is dominated by four different failure modes, i.e. flexure failure, anchorage failure, shear compression failure and shear tension

failure. The design of hollow core slabs is governed by Canadian concrete design code, it is based on ACI (American Concrete Institute) 318 requirements. Because it is very difficult to place stirrups in most manufacturing processes, the hollow core slabs rely on the tensile strength of concrete to resist shear force. The nominal shear strength provided by concrete (web shear cracking strength) is given in ACI 318 by the lesser of Eq. (1.1) or (1.2):

$$V_{ci} = 0.6\sqrt{f'_c}\, b_w d + V_d + \frac{V_i M_{cr}}{M_{max}} \qquad (1.1)$$

$$V_{cw} = (3.5\sqrt{f'_c} + 0.3 f_{pc}) b_w d_p + V_p \qquad (1.2)$$

where V_{ci} is the nominal shear strength of concrete in a shear-flexure failure mode;

V_{cw} is the nominal shear strength of concrete in a web shear failure mode;

f'_c is the specified design compressive strength of concrete;

f_{pc} is the compressive stress in concrete at the centroid of the section due to effective prestress for non –composite sections;

b_w is the net web width of hollow core slab;

d_p is the distance from extreme compression fiber to centroid of tension reinforcement;

d is the distance from extreme compression fiber to centroid of tension reinforcement;

V_d is the shear due to unfactored load;

M_{cr} is the cracking moment;

M_{max} is the maximum factored moment due to externally applied loads.

Figure 1.2 shows a typical hollow core slab cross-section

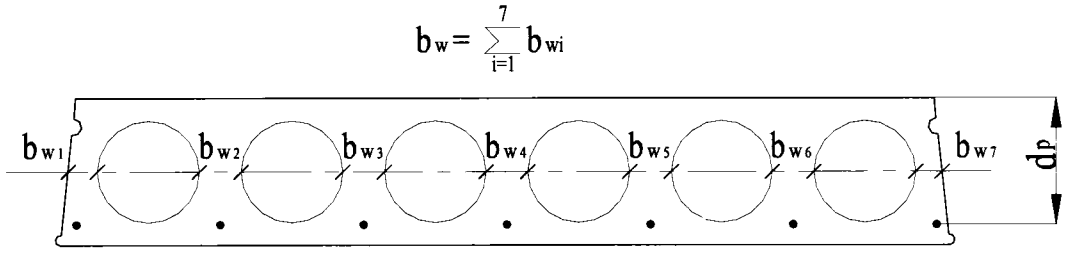

Figure 1.2: Typical cross-section of Hollow Core Slab.

When determining the net web width (b_w), the current practice recommended by ACI 318 code simply sums up the minimum parts of the web (as shown in Figure 1.2) and ignores the interaction between the adjacent webs and flanges. Therefore, when calculating the nominal shear strength, the effective net web width b_w might be underestimated by the current design code. To find out whether the hollow core slab shear strength predicted by ACI 318 code is conservative or not, one possible way is to develop a numerical model that can simulate the structural behavior of the prestressed concrete hollow core slab. The shear capacity of the slab can be obtained from the numerical analysis, based on which the effective web width of hollow core slab can be derived.

Cabrielsson [1] conducted a series of experiments to investigate the ductility of prestressed hollow core slabs subjected to bending, shear and torsion. By reviewing the experimental results of Cabrielsson's web tests and slab tests, it is quite obvious that a

slab has more shear resistance per unit length as compared to a web beam. One possible explanation could be that the boundary conditions of the web beam and the web section in a slab are different. The web beam has no restraints in the flange section while the web in a slab has some interaction with the surrounding webs through flange. Figure 1.3 shows the typical cross-section of a web beam and a hollow core slab.

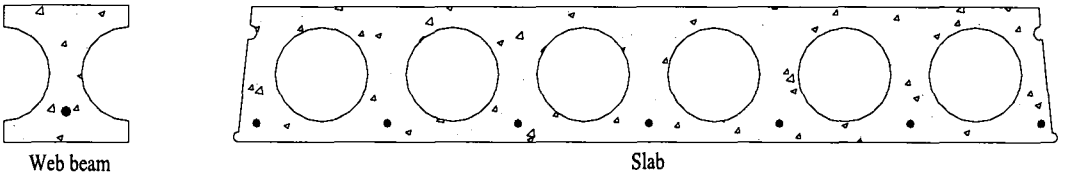

Figure 1.3: Typical cross-section of web beam and Hollow Core Slab.

1.1.1 Classical Analysis for Concrete Structure

Classical beam theory for reinforced and prestressed concrete design is mainly based on linear elastic models, which assumes that plane sections remain plane throughout the loading history. Because of this, the classical beam theory is not capable of dealing with problems where material non-linearity and/or geometric non-linearity exist. Some reinforced concrete T-beams were tested at Empa Materials Science and Technology (Deuring [2]). The deflection and the failure mode of the beams were analysed using the classical beam theory. Results show that in general the load-deflection curves could be predicted by the classical theory with reasonable accuracy. However, while it was predicted by the classical theory that the beams would fail in tension, such a phenomenon was not observed on any of the beams, all the beams failed in compression. In addition,

in the experiment, the concrete compressive strain of the beams at failure varied from 0.19–0.25%, whereas in the classical beam theory a strain of 0.35% is normally used at compression failure of concrete.

Between 1978 and 1987, Yang [3] investigated the web-shear behaviour of 59 simply supported hollow core slabs. The tests were conducted in the Technical Research Centre of Finland (VTT). The overall depths of the units ranged from 7.5 in. (190 mm) to 16.0 in. (410 mm). Most units had a length of 24 ft. Figure 1.4 shows the typical cross-sections of the hollow core slabs used in Yang's tests.

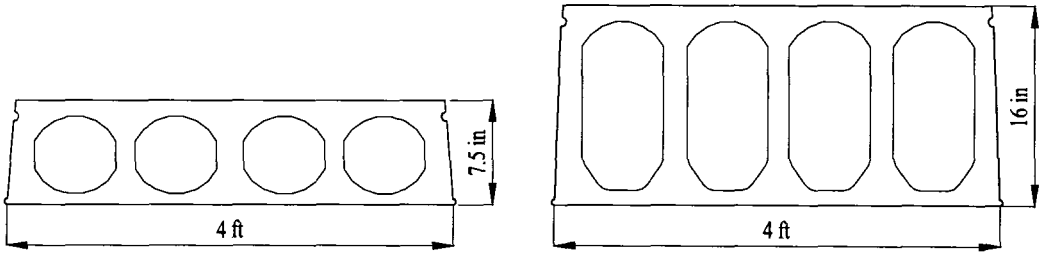

Figure 1.4: Typical cross-section of hollow core slabs in Yang's tests [3].

Through these tests, Yang found that the flexure-shear strength of the specimens obtained in the tests agreed reasonably well with that predicted by the Eurocode. However, the web shear strengths obtained from experiments showed considerable scatter as compared to those by code prediction. Yang also observed that the rate at which the prestressing force was transferred to the concrete within the transfer length could significantly affect the web-shear strength. Web-shear cracking occurred when the principal tensile stress in

the units (at the intersection of the narrowest web and the bottom flange) reached the tensile strength of the concrete for a location on a line drawn from the centreline of the support at an angle of 35 degrees to the axis of the unit. Figure 1.5 shows the failure pattern of Yang's specimen.

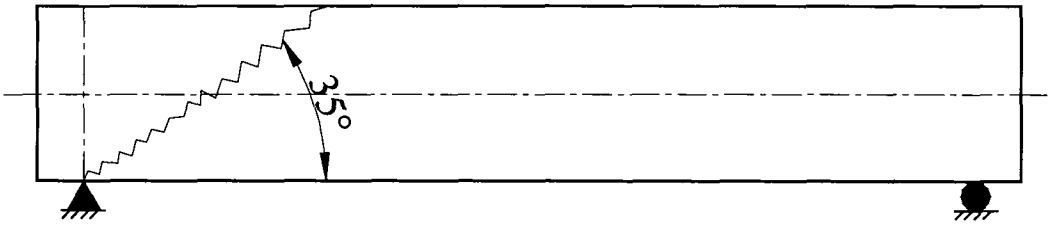

Figure 1.5: Failure pattern of Yang's specimen.

Matti Pajari [4] examined 49 test results on hollow core slabs due to web shear failure made by the Technical Research Centre of Finland (VTT). The height of hollow core slabs ranged from 7.9 in. (200 mm) to 19.7 in. (500 mm) and the length ranged from 16.4 ft. (5010 mm) to 23.6 ft. (7200 mm). The void shape of the slabs in the above tests included both circular void (similar to Figure 1.2) and non-circular void (similar to Figure 1.4). Pajari compared measured strengths with those calculated using Eurocode 2 (EC2) and Yang' s model. The EC2 method overestimated the mean shear strength for all slab types (circular void and non-circular void). While the overestimation was only slight for slabs with circular voids, it was obvious for units with flat webs. For units with flat webs and depths equal to or greater than 10.4 in. (265 mm), strengths were in reasonable agreement with those calculated using Yang' s model.

From Deuring, Yang and Pajari's work it can be seen that the classical concrete beam theory is not suitable for analyzing the concrete structures because of the nonlinear property of the concrete material. On the other hand, though the results from the experimental work are acceptable, it requires a large number of specimens to ensure the quality of the testing data.

1.1.2 Finite Element Analysis for Concrete Structures

The finite element method is a powerful numerical technique for the analysis of non-linear engineering problems. Two simply supported reinforced concrete beams with symmetrically placed concentrated transverse loads (as shown in Figure 1.6) were modeled by Faherty [5] using finite element method. He studied the non-linear concrete properties, linear bond-slip relation, bilinear steel properties, and the influence of progressive cracking of the concrete. Compared with experimental results, his finite element model produced very good results.

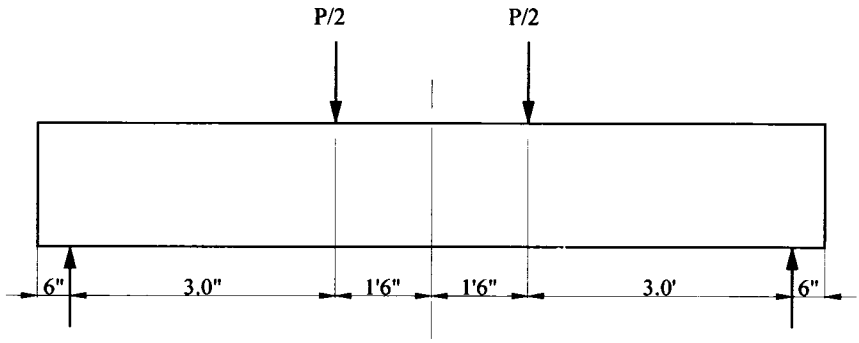

Figure 1.6: Reinforced concrete beam (Faherty [5])

In 2001, Kachlakev [6] used ANSYS to study concrete beams with externally bonded Carbon Fiber Reinforced Polymer (CFRP) fabric. He used eight-node solid element, Solid65, to model the concrete and Link8 element to model the steel reinforcement. The beam dimensions are shown in Figure 1.7.

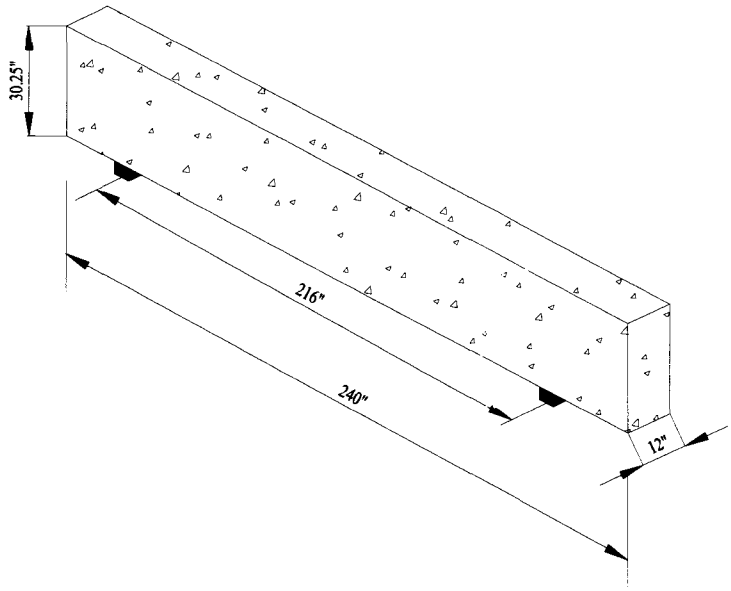

Figure 1.7: Typical beam dimensions used by Kachlakev

Because of symmetry, only one quarter of the beam was modeled as shown in Figure 1.8.

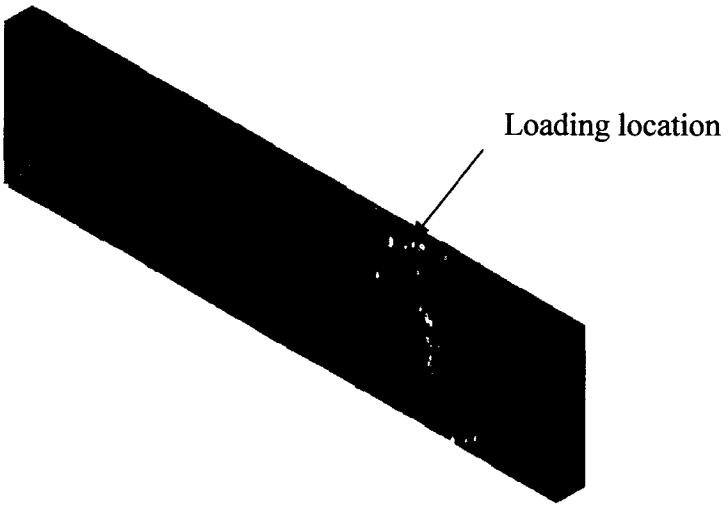

Figure 1.8: Finite element discretization for a quarter of Beam (Kachlakev [6])

A one-inch thick steel plate, modeled using Solid45 elements, was added at the support location in order to avoid stress concentration. This would provid a more even stress distribution over the support area. Moreover, a single line support was placed under the centreline of the steel plate to allow rotation of the plate. Figure 1.9 illustrates the steel plate at the support and loading location.

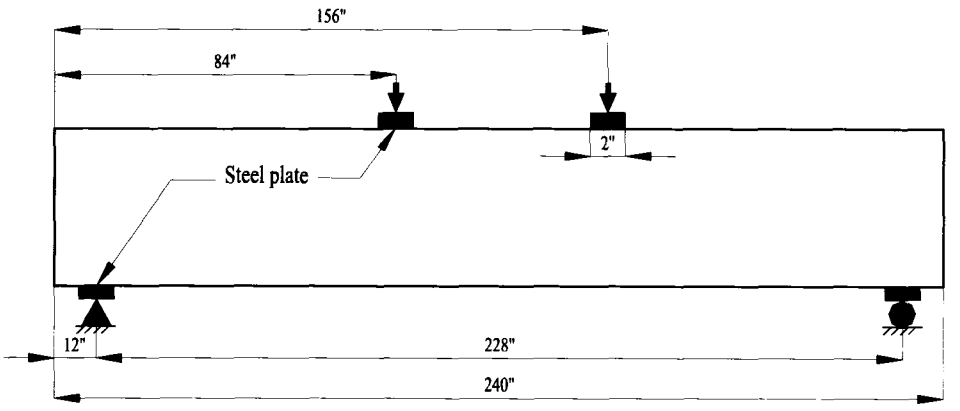

Figure 1.9: Loading and support locations (Kachlakev [6])

The nonlinear Newton-Raphson approach was utilized to trace the equilibrium path during the load-deformation response. It was found that convergence of solutions for the model was difficult to achieve due to the nonlinear behavior of reinforced concrete material. The load-deflection curve for the reinforced beam was plotted as shown in Figure 1.10. It can be seen that the load-deflection relation from the finite element analysis agrees well with the experimental data for the reinforced concrete beam.

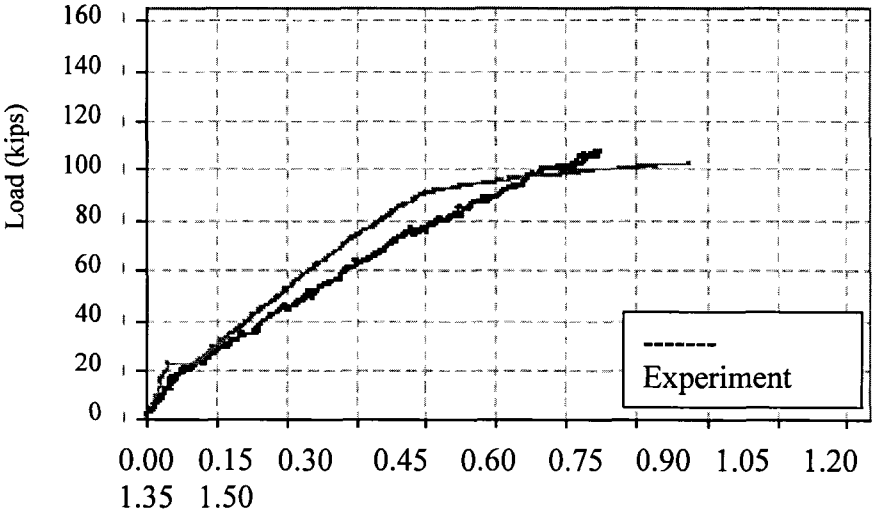

Figure 1.10: Load-deflection plot for the beam (Kachlakev [6])

In 2003, Anthony J. Wolanski [7] studied the flexural behaviour of reinforced and prestressed concrete beams using finite element package - ANSYS 2003. The geometric dimension of the concrete beam was shown in Figure 1.11.

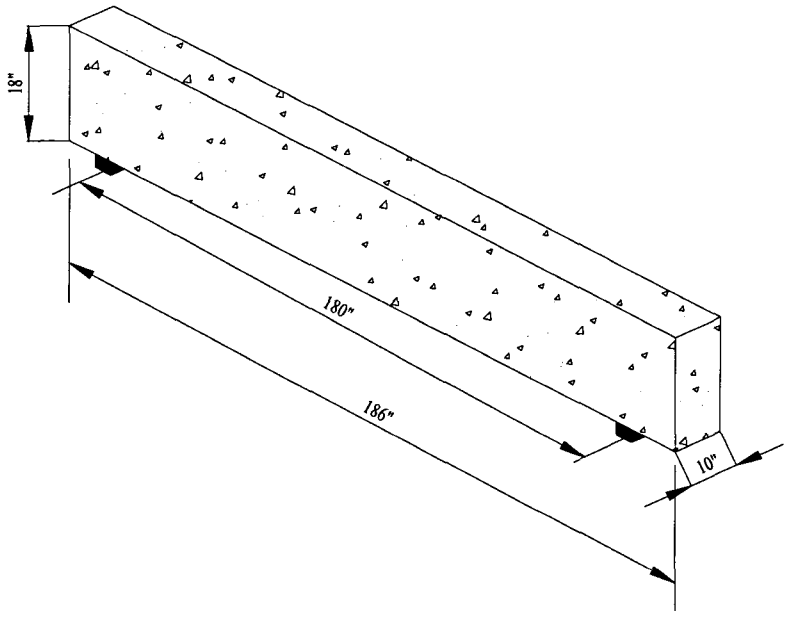

Figure 1.11: Beam dimensions used by Anthony [7]

Three element types: solid65, solid45 and link8 were used to model concrete, steel plate and reinforcing steel, respectively. Because of symmetry, only a quarter of the beams were modeled as shown in Figure 1.12.

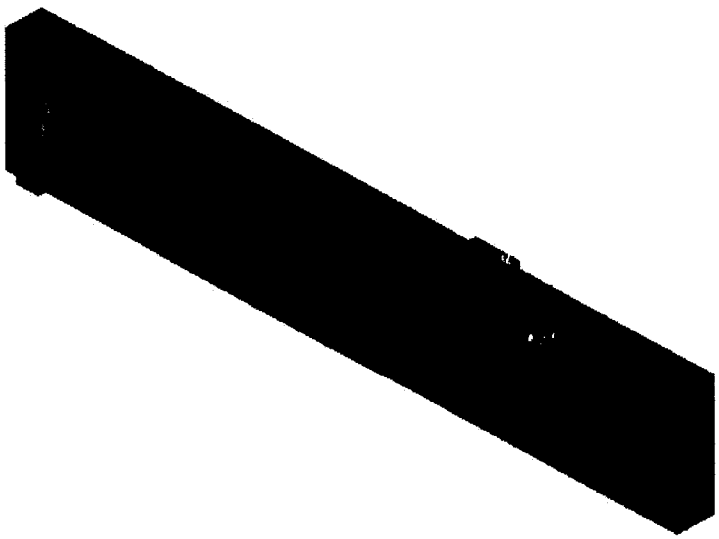

Figure 1.12: FEM model for a quarter of concrete beam (Anthony [7])

Anthony compared his ANSYS analysis results with the experimental data by Buckhouse [8]. It can be seen that the entire load-deflection relation by numerical simulation compares very well with the experimental data. The load-deflection relation at centreline of the beam is shown in Figure 1.13.

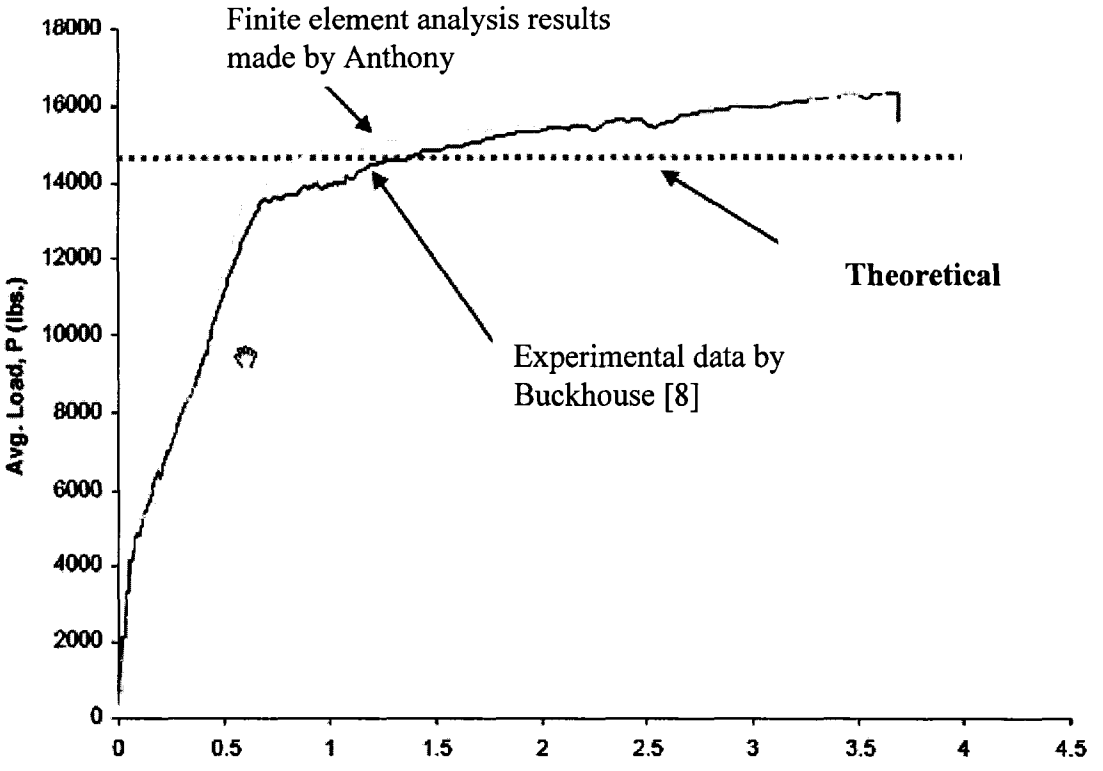

Figure 1.13: Centreline Deflection (Anthony [7])

1.2 Motivations

When determining the shear strength of hollow core slabs, the effective web width could be underestimated by the present ACI 318 code because it neglects any possible interactions between the adjacent webs and flanges, and simply sums up the minimum parts of the slab web, as shown in Figure 1.2. In the experimental work by Cabrielsson [1] to investigate the ductility of prestressed hollow core slabs subjected to bending, shear and torsion, it was found that the slab had higher shear capacity than the web beam. But no further tests and analyses have been done to confirm and quantify it.

We were approached by the local precast concrete industry, the Prestressed System Inc. (PSI) to study the effective web width of hollow core slabs. Being designers, they are eager to know if the effective web width defined in the current ACI code is reasonable or conservative. After reviewing the current research status of the structural behaviour and strength of prestressed hollow core slabs, it was found that research work related to this specific topic was rarely available in the literatures. Therefore, it is necessary to conduct further study to clarify this issue. A straight way to evaluate the strength of concrete member is through experimental work, but the cost is relatively high. Compared with the experimental tests, the finite element analysis method is time efficient and much cheaper. From the literature review it can be seen that using finite element method to model reinforced concrete beam is viable and the results obtained from the model are compared reasonably well with the experimental data. In the current study, the shear behaviour of prestressed hollow core slabs will be examined both numerically and experimentally. It is expected that the results from the present work will serve as a paving stone, which will lead to more quantitative studies on this topic and contribute to the refinement of the existing code.

1.3 Objectives

The objectives of the proposed research are as follows:

1) To derive a finite element based numerical model for prestressed hollow core slabs under shear force. The model will be developed using commercial finite element package ANSYS 2003.

2) To verify the proposed numerical model. The load-deflection diagram will be obtained from the numerical simulation and it will be compared with the experimental data.

3) To verify the parameters of element in the numerical model. Three types of element will be used in this model: Solid65, Link8 and Solid45. There are more than 20 parameters in these elements. The crucial ones include the shear transfer coefficients for an open (or closed) crack, the uniaxial tensile cracking strength and uniaxial crushing strength.

4) To obtain the maximum shear capacity of hollow core slabs and reinforced concrete I-shaped beams through physical tests.

5) To evaluate the effective web width (b_w) for hollow core slabs used in the current ACI design code.

CHAPTER 2 Nonlinear Finite Element Modeling

2.1 Specimens

Two groups of specimens are used in this study. The first group includes four same I-shaped prestressed concrete beams (cut from the hollow core slabs); while the second includes four same full size hollow core slabs. They were fabricated by the Prestressed Systems Inc. (PSI) located in Windsor and tested at the Structures Lab at the University of Windsor. As shown in Figure 2.1 (a), the length of a typical specimen was 180 in. (4570 mm) with supports located 3.35 in. (85 mm) from each end of the specimen allowing a simply supported span of 173 in. (4400 mm). Figure 2.1 (b) shows the cross section of the prestressed concrete beam. It can be considered as a single web hollow core slab because it was cut from a hollow core slab. The cross section of the hollow core slab specimen is illustrated in Figure 2.1 (c).

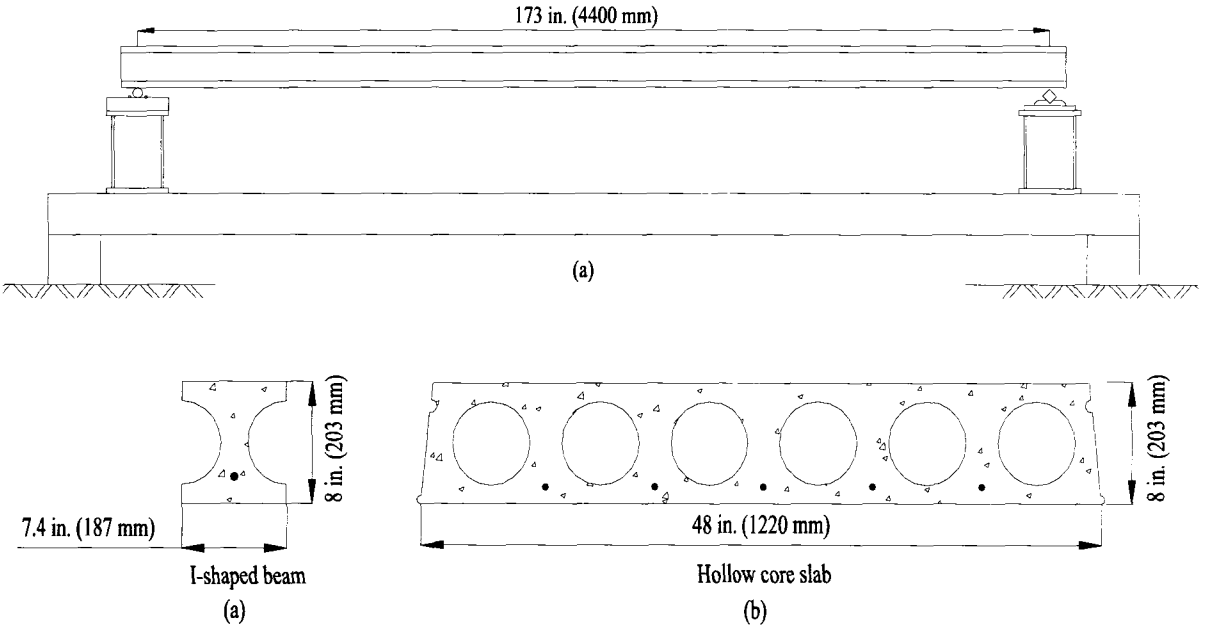

Figure 2.1: Elevation and cross sections (a) Elevation of beam and slab (b) Cross section of beam (c) Cross section of slab

Figure 2.2 and Figure 2.3 show the experimental set-up of an I-shaped beam and a hollow core slab in the structures lab at the University of Windsor, respectively.

Figure 2.2: Experimental set-up of an I - shaped beam

Figure 2.3: Experimental set-up of a Hollow Core Slab

In the following sections, the four beams will be referred to as "Beam-1" to "Beam-4" and the four slabs will be referred to as "Slab-1" to "Slab-4". Table 1 shows the dimension and loading location of each specimen.

Table 2.1: Dimension and loading location of specimens

	Length, in. (mm)	Depth, in. (mm)	Shear span, in. (mm)
Beam-1	180 (4570)	8 (203)	23.6 (600)
Beam-2	180 (4570)	8 (203)	33.5 (850)
Beam-3	180 (4570)	8 (203)	27.6 (700)
Beam-4	180 (4570)	8 (203)	19.7 (500)
Slab-1	180 (4570)	8 (203)	23.6 (600)
Slab-2	180 (4570)	8 (203)	33.5 (850)
Slab-3	180 (4570)	8 (203)	27.6 (700)
Slab-4	180 (4570)	8 (203)	19.7 (500)

All the specimens have one roll support and one pin support which leads to a simply supported beam. One dial gauge is attached to the top center of the specimen at mid-span to measure the deflection. The load is applied slowly in a number of steps till failure by a universal loading machine with a maximum loading capacity of 67.5 kips [300 kN]. The model number of the loading cell is FL100U(C)2SGKT. Strain gauges are attached to the side and top of Beam-2 to record the structural shear behaviour under concentrated load.

2.2 Element Types

The finite element program ANSYS 2003, operating on a Windows XP platform is used in this study to simulate the behaviour of the prestressed I-shaped beams and hollow core

slabs. Three types of elements are used in this study; i.e., SOLID65, LINK8, and SOLID45 to model concrete, prestressed reinforcing steel bars and steel plate, respectively. The material properties defined for each type of element in the finite element model are based on the standard test made by FSI.

2.2.1 Concrete

Solid65 element is used to model the concrete. This element is capable of cracking in tension and crushing in compression. It also has the property of plastic deformation and creep. The most important aspect of this element is the treatment of non-linear material properties. Solid65 element has eight nodes with three degrees-of-freedom at each node, i.e. translations in the nodal x, y, and z directions. The geometry and node locations of this element type are shown in Figure 2.4.

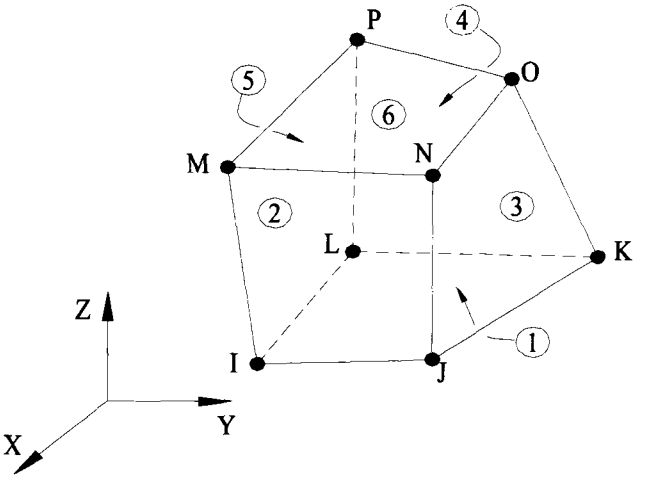

Figure 2.4: Solid65 element (ANSYS 2003)

2.2.2 Reinforcement

Link8 element is used to model the prestressed steel reinforcement. This 3-D spar element is a uniaxial tension-compression element with three-degrees-of freedom at each nodal end, "I" and "J", i.e. translations in the nodal x, y, and z directions. Two nodes are required for this element. The element is also capable of modeling plastic deformation. The geometry and node locations of this element type are shown in Figure 2.5.

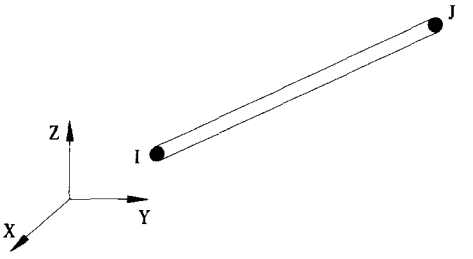

Figure 2.5: Link8 element (ANSYS 2003)

2.2.3 Steel plate

Another type of eight-node solid element, Solid45, is used for the steel plates at the top in the beam models where the load will be applied. The element has plasticity, creep, swelling, stress stiffening, large deflection, and large strain capabilities. The biggest difference between solid45 and solid65 is that the former does not have the ability to crack and crush. This element is defined by eight nodes with each node having three-degrees-of freedom at each node-translations in the nodal x, y, and z directions. The geometry and node locations of this element type are shown in Figure 2.6.

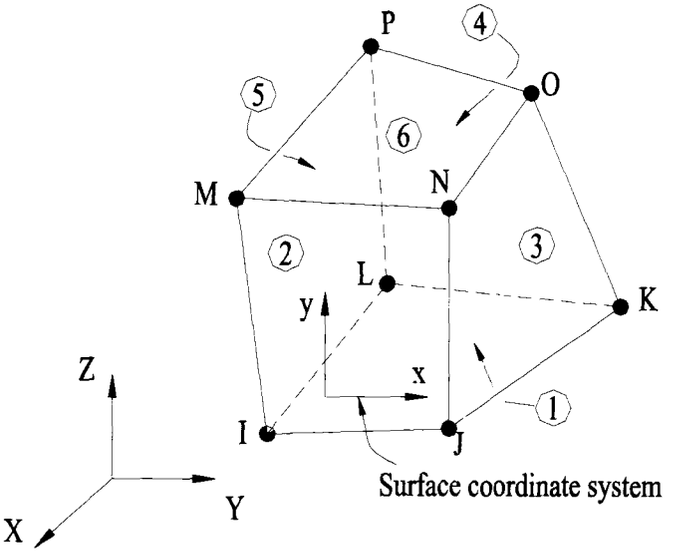

Figure 2.6: Solid45 element (ANSYS 2003)

2.3 Material Properties

2.3.1 Concrete

Concrete is a mixture of cement paste and aggregates. Its stress-strain relation is non-linear and appears to be somewhat ductile. As a quasi-brittle material, concrete has very different behaviour in compression and tension. Usually the tensile strength of concrete varies from about 8 - 15% of its compressive strength. A major reason for this low tensile strength is the fact that concrete is filled with fine cracks. When concrete is subjected to compressive load, because the cracks would close under the compressive stress and allow it to be transferred, the cracks would have little impact on the concrete compressive strength. Obviously, this is not the case when tensile load is applied. Figure 2.7 shows a typical stress-strain relation curve of normal weight density concrete (Bangash [9]).

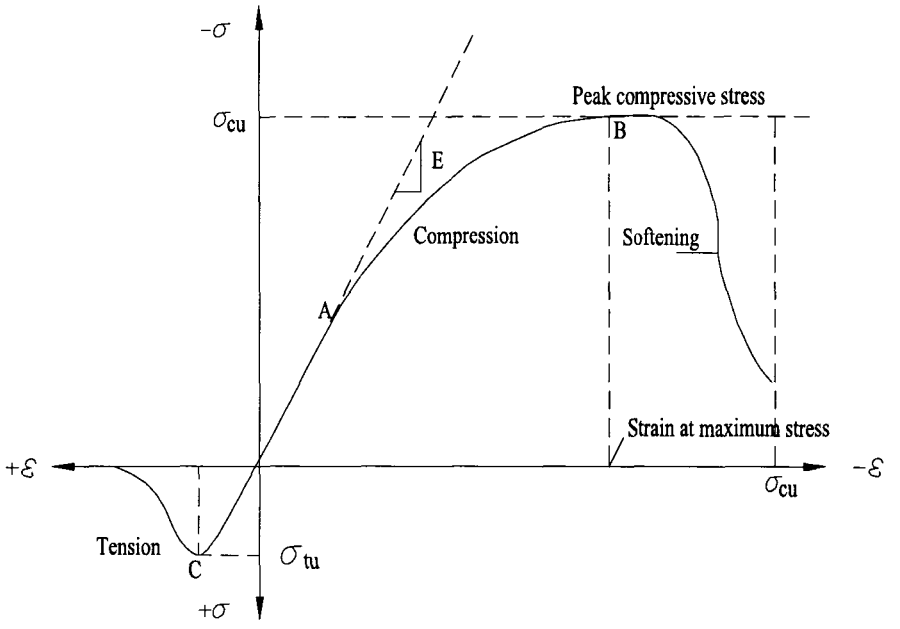

Figure 2.7: Typical uniaxial compressive and tensile stress-strain curve of normal weight density concrete (Bangash [9])

In the compression zone, the stress-strain curve of concrete is linearly elastic up to about 30% of the maximum compressive strength (point A). Beyond point A, the stress goes into non-linear range, increases gradually up to the maximum compressive strength (point B). After it reaches the maximum compressive strength σ_{cu}, the curve descends into a softening region, and eventually crushing failure occurs at an ultimate strain ε_{cu}. In the tension zone, the stress-strain curve of concrete is approximately linearly elastic up to the maximum tensile strength σ_{tu} (point c). Beyond point C, the concrete cracks and the tensile strength decreases gradually to zero (Bangash [9]).

2.3.1.1 Input data used in the finite element model

The input data of concrete material properties required by ANSYS are listed in Table 2.2. They will be explained in the following sections.

Table 2.2: Material Models of the Beam

Element Type	Material Properties		
Solid65	Linear Isotropic		
	EX	4413 ksi (30.43 Mpa)	
	PRXY	0.19	
	Multilinear Isotropic		
		Strain	Stress, psi (Mpa)
	Point1	0	0
	Point2	0.0004	1766 (12.18)
	Point3	0.0006	2430 (16.75)
	Point4	0.0012	4351 (30.00)
	Point5	0.0016	5374 (37.05)
	Point6	0.002	6000 (41.37)
	Point7	0.0022	5816 (40.10)
	Point8	0.0024	5374 (37.05)
	Point9	0.0028	4351 (30.00)
	Concrete		
	ShrCf-Op	0.3	
	ShrCf-Cl	0.95	
	UnTensSt	580 psi (4.0 MPa)	
	UnCompSt	6000 psi (41.37 MPa)	
	BiCompSt	0	
	HydroPrs	0	
	BiCompSt	0	
	UnTensSt	0	
	TenCrFac	0	

The Solid65 element requires linear isotropic and multilinear isotropic material properties to properly model the behaviour of concrete material. The multilinear isotropic material uses the Von Mises failure criterion along with the Willam and Warnke [10] model to define the failure of the concrete. The Willam and Warnke model is defined as follows: Cracking is permitted in three orthogonal directions at each integration point. If cracking occurs at an integration point, the cracking is modeled through an adjustment of material properties which effectively treats the cracking as a "smeared band" of cracks, rather than discrete cracks. The concrete material is assumed to be initially isotropic. In addition to cracking and crushing, the concrete may also undergo plasticity, the plasticity is done before the cracking and crushing checks.

Modulus of elasticity (EX):

EX is the modulus of elasticity of the concrete, which is usually designated by Ec. In the case of normal weight concrete, ACI section 8.5.1 recommends to use the following empirical formula:

$$E_c = 57000 \sqrt{f_c'} \qquad (2.1)$$

where f_c' is the specified compressive stress of concrete. According to the standard test made by PSI, the specified compressive stress of concrete is 6000 psi [41.37 Mpa]. A value of 6,000 psi (41.37 Mpa) would correspond to a E_c of 4415 ksi (30,443 MPa).

Possion's ratio (PRXY):

PRXY is the Poisson's ratio γ of the concrete. The Possion's ratio of concrete various from about 0.11 to 0.2 and usually falls in the range of 0.15 to 0.20. Based on the testing results of biaxially loaded concrete, Kupfer [11] reported values of 0.20 for the Possion's ratio of concrete loaded in compression in one or two directions, 0.18 for concrete loaded in tension in one or two directions, and 0.18 to 0.20 for concrete loaded in tension and compression. Possion's ratio remains approximately constant under sustained load. In this study, the concrete is under both tension and compression, so 0.19 was selected as Possion's ratio of concrete.

The compressive uniaxial stress-strain relationship of the concrete model was obtained from ACI code [13]. The implementation of the multilinear isotropic stress-strain curve requires that the first point on the curve to be defined by the user. It must satisfy the Hooke's Law, i.e.

$$E = \frac{\sigma}{\varepsilon} \qquad (2.2)$$

The multilinear curve was used to help with convergence of the nonlinear solution.

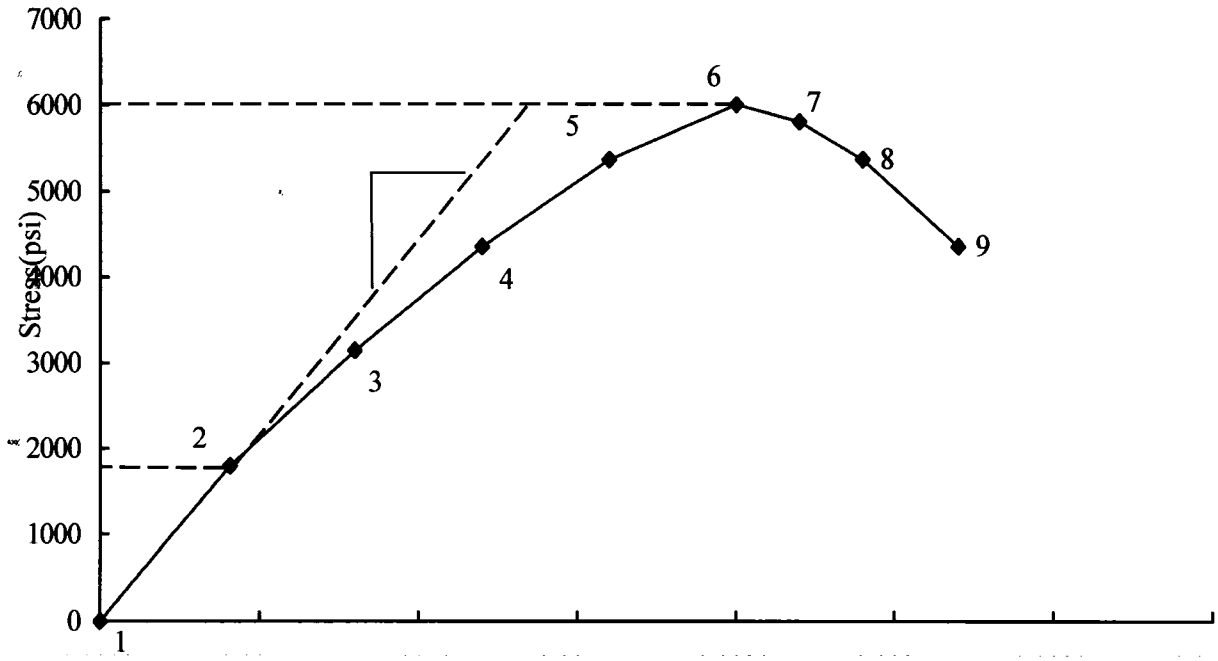

Figure 2.8: Uniaxial Stress-Strain Curve

Figure 2.8 shows the concrete stress-strain relationship used in this study, it is based on ACI 318-05 Code [13]. Point 2, defined as 0.30 $f_c^{'}$, is calculated in the linear range by using Eq. (2.2). Points 3 to 9 are obtained from reference [13].

Material model:

The material model in ANSYS is from Willam and Warnke [10], it requires that 9 different constants to be defined. These 9 constants are listed in Table 2.3. The failure criteria of this model will be explained in the following section.

Table 2.3: Concrete material data in ANSYS

Constant	Parameter
1	Shear transfer coefficients for an open crack
2	Shear transfer coefficients for a closed crack.
3	Uniaxial tensile cracking stress.
4	Uniaxial crushing strength (positive).
5	Biaxial crushing strength (positive).
6	Ambient hydrostatic stress state for use with constants 7 and 8.
7	Biaxial crushing stress (positive) under the ambient hydrostatic stress state (constant 6).
8	Uniaxial crushing stress (positive) under the ambient hydrostatic stress state (constant 6).
9	Stiffness multiplier for cracked tensile condition.

Shear transfer coefficient (constant 1 and 2):

Shear transfer coefficient of concrete varies from 0.0 to 1.0, with 0.0 representing a smooth crack (complete loss of shear transfer) and 1.0 representing a rough crack (no loss of shear transfer). A number of preliminary analyses were attempted in this study with various values of the shear transfer coefficient within this range, but convergence problems were encountered when shear transfer coefficient was taken as less than 0.5. Therefore, the shear transfer coefficient for an open crack used in this study was chosen to be 0.3. For the same reason, the shear transfer coefficient for a closed crack was set to be 0.95 (Table 2.1).

Uniaxial tensile cracking strength (constant 3):

Although tensile strength is normally neglected in most reinforced concrete design calculations, it is not the case for the shear capacity calculation of hollow core units. Because there are no stirrups in the hollow core unit, its shear capacity mainly depends on the tensile strength of concrete. The tensile strength of concrete does not vary in proportion to its compressive stress $f_c^{'}$. It does, however, vary approximately in proportion to the square root of $f_c^{'}$. Based on hundreds of tests, the ACI Code [13] (section 9.5.2.3) recommends that the uniaxial tensile cracking strength could be considered the same as the modulus of rupture of concrete, f_r, i.e.

$$f_r = 7.5\sqrt{f_c^{'}} \tag{2.3}$$

where $f_c^{'}$ and f_r are in "psi".

Uniaxial crushing strength (constant 4)

The uniaxial crushing strength was determined based on the uniaxial compressive strength ($f_c^{'}$). In this model, it was taken as the same value as $f_c^{'}$. The remaining variables in the concrete model used the default values given in the ANSYS software.

2.3.1.2 Failure Criteria for Concrete

The concrete material model predicts the failure of brittle materials. Both cracking and crushing failure modes are considerd. The criterion for failure of concrete due to a multiaxial stress state can be expressed in the form below (Willam and Warnke [10]):

$$\frac{F}{f_c} - S \geq 0 \tag{2.4}$$

where F = a function of the principal stress state ($\sigma_{xp}, \sigma_{yp}, \sigma_{zp}$)

$\sigma_{xp}, \sigma_{yp}, \sigma_{zp}$ = principal stresses in the principal directions X, Y and Z

S = failure surface (to be discussed) expressed in terms of principal stresses and five input parameters f_t, f_c, f_{cb}, f_1 and f_2.

f_t = ultimate uniaxial tensile strength

f_c = uniaxial crushing strength

f_{cb} = ultimate biaxial compressive strength

f_1 = ultimate compressive strength for a state of biaxial compression superimposed on hydrostatic stress state

f_2 = ultimate compressive strength for a state of uniaxial compression superimposed on hydrostatic stress state

However, the failure surface can be specified with a minimum of two constants, f_t and f_c. The default values of the other three constants used by Willam and Warnke [10] are:

$$f_{cb} = 1.2\, f_c \tag{2.5}$$

$$f_1 = 1.45\, f_c \tag{2.6}$$

$$f_2 = 1.725\, f_c \tag{2.7}$$

The ambient hydrostatic stress state, denoted as σ_h, is defined as:

$$\sigma_h = \frac{1}{3}(\sigma_{xp} + \sigma_{yp} + \sigma_{zp}) \tag{2.8}$$

A three-dimensional failure surface of concrete is shown in Figure 2.9. The most significant nonzero principal stresses are in the x and y directions, represented by

σ_{xp} and σ_{yp}, respectively. Three failure surfaces are shown as projections on the σ_{xp} - σ_{yp} plane. The mode of failure is a function of the sign of σ_{zp}. For example, if σ_{xp} and σ_{yp} are both negative (compressive) and σ_{zp} is slightly positive (tensile), cracking would be predicted in a direction perpendicular to σ_{zp}. However, if σ_{zp} is zero or slightly negative, the material is assumed to be crushed [12].

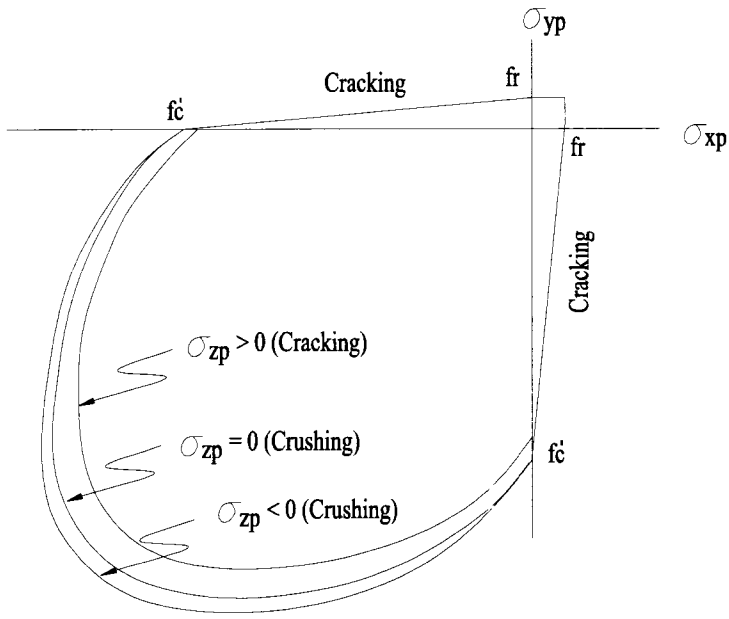

Figure 2.9: 3-D failure surface of concrete [12]

In a concrete element, cracking occurs when the principal tensile stress in any direction lies outside the failure surface. After cracking, the elastic modulus of the concrete element is set to zero in the direction parallel to the principal tensile stress direction. Crushing occurs when all principal stresses are compressive and lies outside the failure surface; subsequently, the elastic modulus is set to zero in all directions [9], and the element effectively disappears. Crushing of the concrete starts to develop in elements

located directly under the loads. Subsequently, adjacent concrete elements crushes within several load steps as well, which significantly reduces the local stiffness. Finally, the model shows a large displacement, and the solution diverges.

2.3.2 Steel Reinforcement and Steel Plate

Link8 element is being used for modeling steel reinforcement. The steel reinforcement in the specimens was prestressed using 7-wire strands which have a diameter of ½ in. (13 mm) and a tensile strength of 270 ksi (1860 MPa). The material property of the prestressed steel was modeled by using a multilinear stress-strain curve developed based on the following equations [13],

$$\varepsilon_{PS} \leq 0.0086 \quad : f_{PS} = 28500 \ \varepsilon_{PS} \ \text{(ksi)} \tag{2.5}$$

$$\varepsilon_{PS} \leq 0.0086 \quad : f_{PS} = 270 - \frac{0.04}{\varepsilon_{PS} - 0.007} \ \text{(ksi)} \tag{2.6}$$

Table 2.4 shows the magnitude stress and strain calculated based on Eq. (2.5) and Eq. (2.6). These data are plotted in Figure 2.10.

Table 2.4: Values for multilinear stress-strain curve of prestressed strand

Strain(mm/mm)	Stress(MPa)	Strain(mm/mm)	Stress(MPa)	Strain(mm/mm)	Stress(MPa)
0	0	0.0107	1724.735	0.0135	1773.997
0.008	1544.48	0.0109	1730.331	0.0137	1776.037
0.0083	1560.568	0.0111	1735.442	0.0139	1777.978
0.0085	1589.298	0.0113	1740.126	0.0141	1779.817
0.0087	1612.803	0.0115	1744.435	0.0143	1781.562
0.0089	1632.391	0.0117	1748.413	0.0145	1783.219
0.0091	1648.965	0.0119	1752.096	0.0147	1784.796
0.0093	1663.173	0.0121	1755.516	0.0149	1786.297
0.0095	1675.485	0.0123	1758.701	0.0151	1787.729
0.0097	1686.258	0.0125	1761.673	0.0171	1791.074
0.0099	1695.765	0.0127	1764.453	0.0189	1806.156
0.0101	1704.214	0.0129	1767.06	0.0215	1813.385
0.0103	1711.775	0.0131	1769.508	0.0259	1821.204
0.0105	1718.579	0.0133	1771.812	0.0301	1825.948

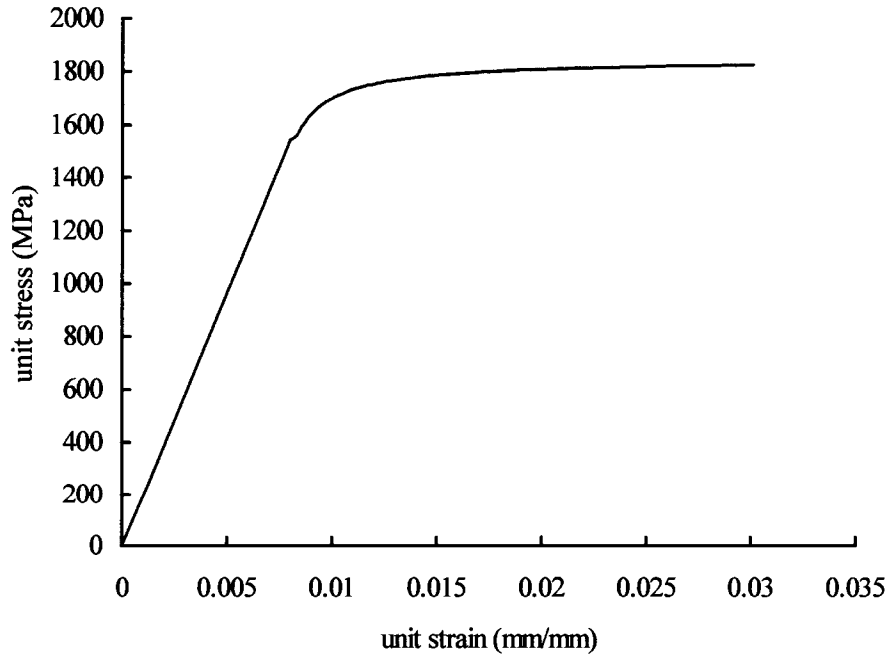

Figure 2.10: Stress-strain curve of prestressed steel strands

The material properties of the prestressed steel strands are taken as follows:

The elastic modulus E_s = 29000 ksi (200,000 Mpa); the Yield strength

f_y = 60,000 psi (414 Mpa); and the Possion's ratio $\gamma = 0.3$.

The material properties of the steel plates in the finite element models were assumed to be perfectly elastic, and the strengths are identical in tension and compression. Since the Solid45 element was used to model the steel plates at loading locations on the beam, this element was modeled as a linear isotropic element with a modulus of elasticity of the steel as E_s = 29000 ksi (200,000 Mpa), and the Possion's ratio $\gamma = 0.3$. Figure 2.11 shows the stress-strain curve of steel plates used in this model.

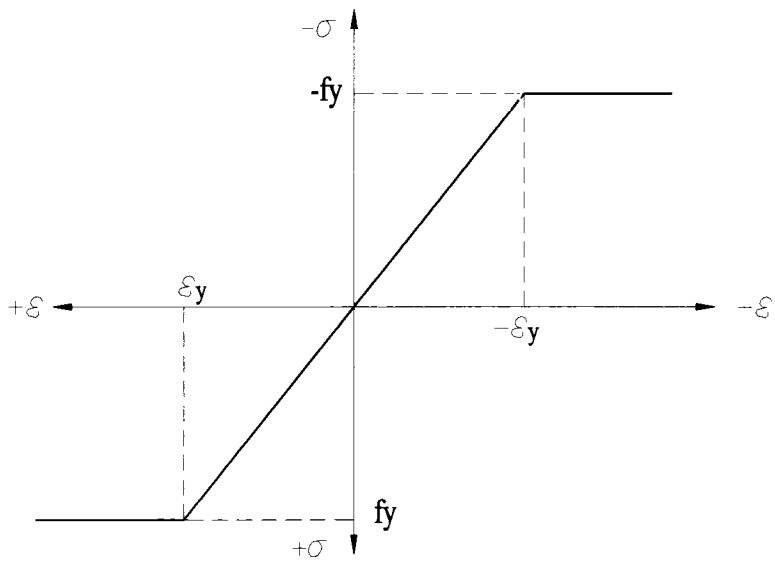

Figure 2.11: Stress-strain curve for steel plate

2.4 Finite Element Discretization

The first step of finite element analysis is to develop mesh for the model. In other words, the model needs to be divided into a number of small elements, so after loading, stress and strain are calculated at integration points of these small elements [14]. One of the important steps in finite element modeling is the selection of the mesh density. Convergence will be obtained when sufficient number of elements is used in the model. This is practically achieved when an increase in the mesh density has a negligible effect on the results [15]. Therefore, a convergence study was carried out to determine an appropriate mesh density for the finite element model.

2.4.1 Finite Element Discretization of Beam Model

Because of symmetry, only half of the beam was simulated using ANSYS 2003. Therefore, a 3.7 in. (93.5 mm) x 8 in. (203 mm) x 173 in. (4400 mm) prestressed concrete beam was analysed. Four different mesh sizes of 528, 1056, 1936 and 3872 elements, respectively, were used to examine the convergence of the results. Three parameters, i.e. the maximum deflection, the maximum compressive stress in the concrete and the maximum tensile stress in the steel reinforcement were monitored to determine if the results converged or not. Figure 2.12 and Table 2.5 show the results of the convergence study.

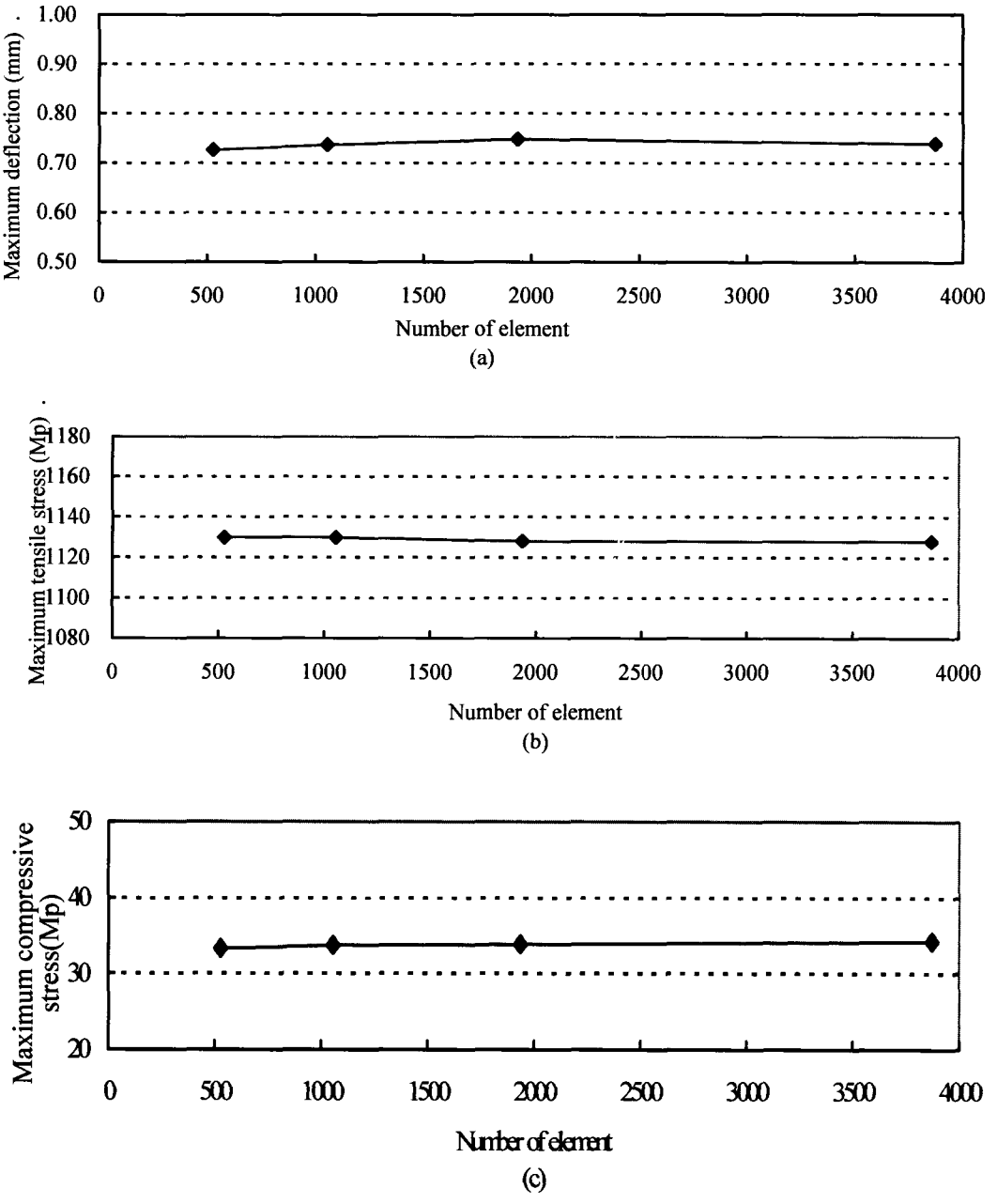

Figure 2.12: Results from convergence study: (a) Maximum deflection; (b) Maximum tensile stress in steel reinforcement; (c) Maximum compressive stress in concrete

Table 2.5: Comparisons of results in the convergence study

Number of elements	Maximum deflection		Tensile stress		Compressive stress		CPU time	
	Magnitude (mm)	Difference %	Magnitude (Mpa)	Difference %	Magnitude (Mpa)	Difference %	Magnitude (s)	Difference %
528	0.726	0.0	1130.1	0.0	33.4	0.0	93	0.0
1056	0.737	1.5	1130.2	0.0	33.8	1.2	158	69.9
1936	0.748	3.0	1128.2	0.2	33.9	1.5	399	329.0
3872	0.738	1.6	1128.0	0.2	34.3	0.3	630	577.4

Note: All the differences are based on the result of element size 528.

From Figure 2.12 and Table 2.5 we can see that the differences in the results were very small when the number of elements increased from 528 to 3872, however, the calculation time increased dramatically at the same time. Therefore, to shorten the calculation time, the 528 element model was selected for the Beam model and used as the base for the other specimens as well.

The beam and plate were modeled as volume elements. The finite element mesh for the beam model is shown in Figure 2.13.

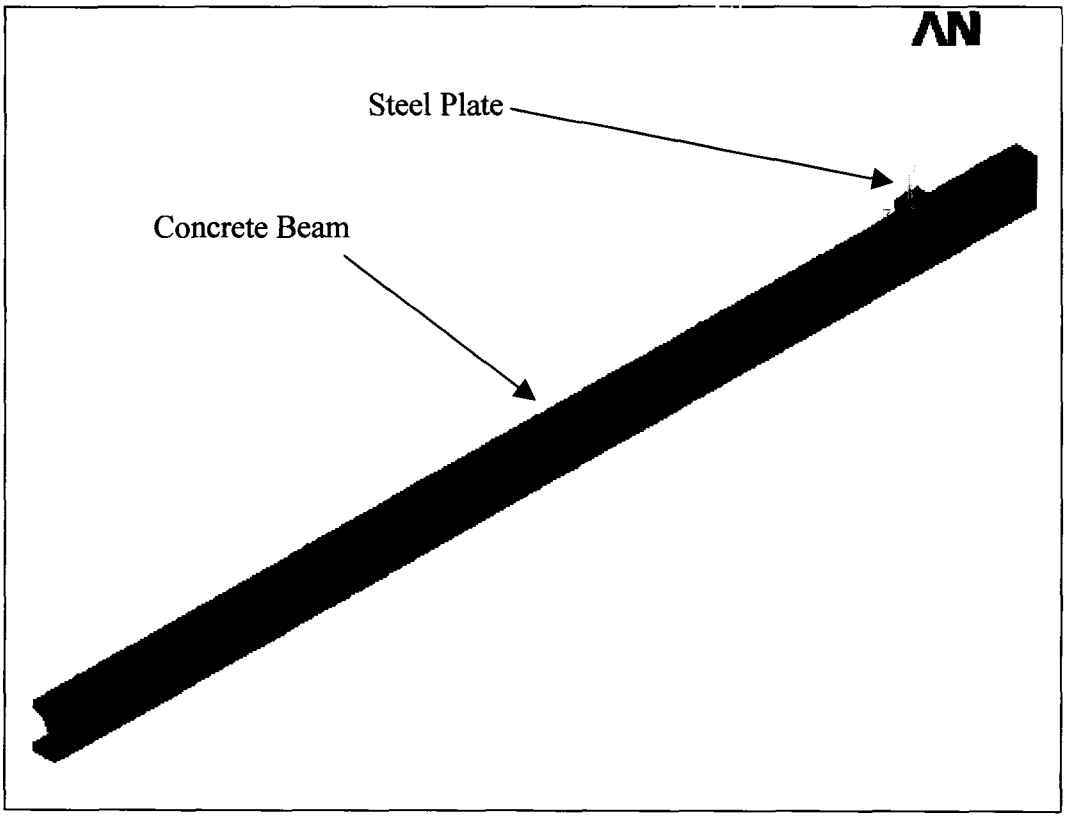

Figure 2.13: The finite element meshes of the beam model

The Link8 element was used to model the prestressed reinforcement. Reinforcement locates at the plane of symmetry about vertical axis in the beam. Thus, the area of steel at the plane of symmetry is one half of the normal area.

2.4.2 Finite Element Discretization of Slab Model

For the slab model, only 1/12 of the slab was modeled because of geometric symmetry. The element type and mesh size of the hollow core concrete slab model are the same as those in the beam model. Figure 2.14 shows the finite element mesh for the slab model.

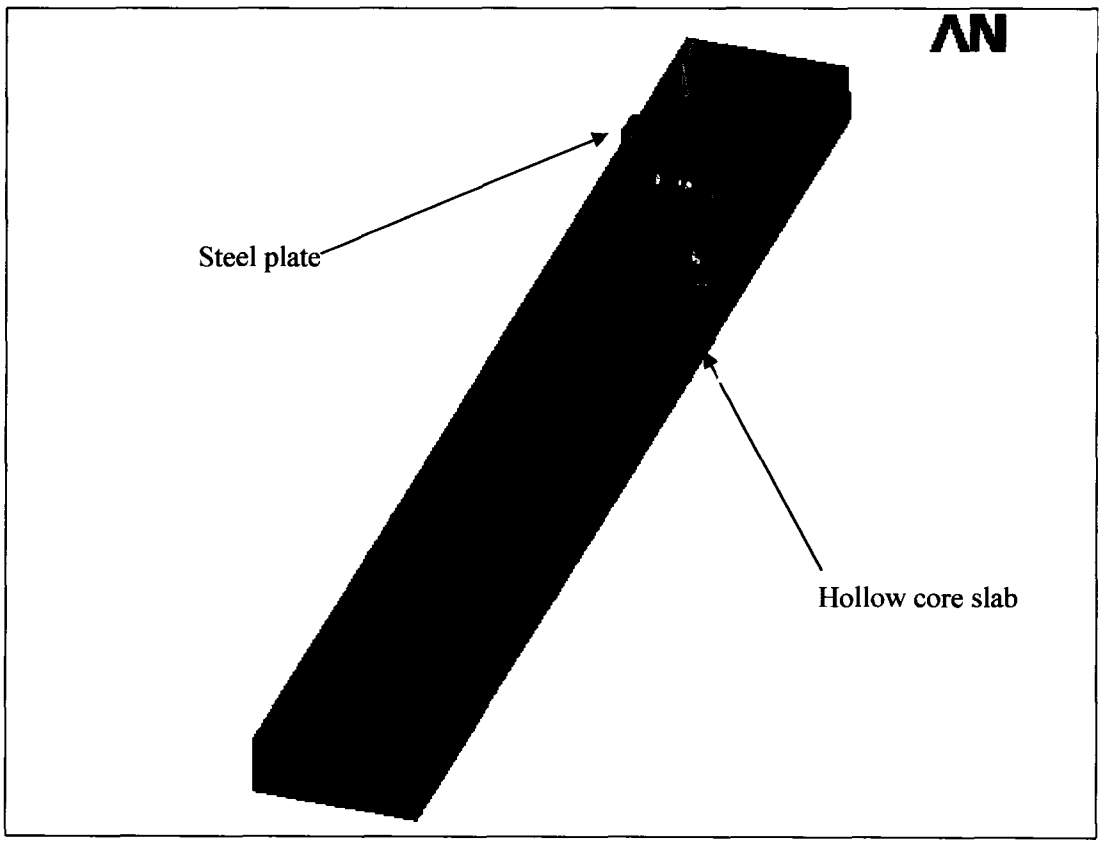

Figure 2.14: The finite element meshes of the slab model

2.5 Loading and Boundary Conditions

2.5.1 I-shaped beams

a) Modeling of boundary conditions

Four beams were tested for shear strength under concentrated load. The finite element models were loaded at the same locations as the tested beams. A steel plate, 1.97 in. (50 mm) thick, 3.94 in. (100 mm) wide), modeled using Solid45 elements, was added at the loading area in order to avoid stress concentration problems in the numerical simulation.

This provided a more even stress distribution over the loading area. Figure 2.15 illustrates the boundary conditions and loading position of the specimen. The distance L from the support to the loading point (shear span) were taken as 19.7 in. (500 mm), 23.6 in. (600 mm), 27.6 in. (700 mm) and 33.5 in. (850 mm) respectively in the four beams.

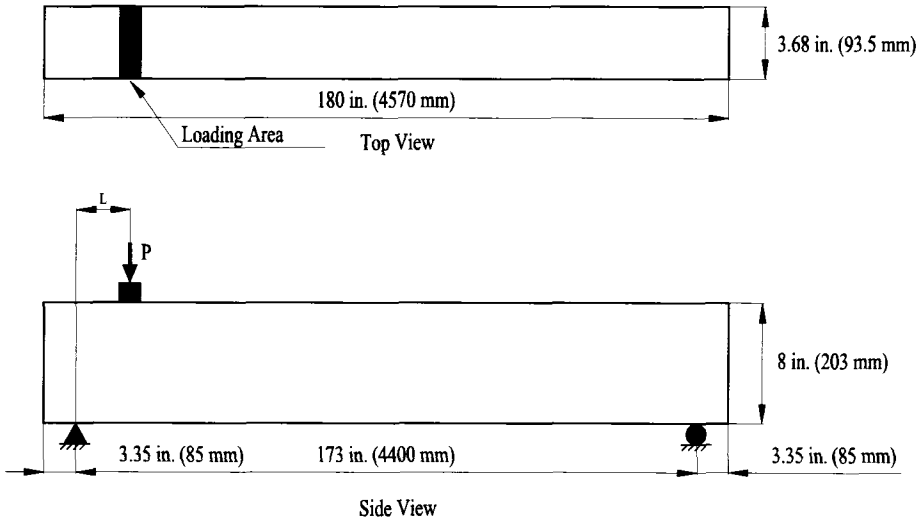

Figure 2.15: Boundary conditions and loading position of the specimen.

Displacement boundary conditions are required to constrain the model so that a unique solution can be obtained. To ensure that the model acts the same way as the experimental beam, boundary conditions need to be applied at points of symmetry, and locations of the supports and loading.

The symmetric boundary conditions were set first. In the finite element model, the directions of the X, Y and Z-axis were defined as follows: the Z-axis was set along the longitudinal direction of the beam, the X-axis was set in the horizontal plane and

perpendicular to the longitudinal axis of the beam and the Y-axis was set in the vertical plane and perpendicular to the X-axis and Z-axis.

The model being used is symmetric about the YZ plane (along the axis of the beam, shown in Figure 2.15). To model the symmetry, nodes on this plane must be constrained in the transverse direction. These nodes, therefore, have a displacement constraint along X-axis as zero. Figure 2.16 shows the boundary conditions when YZ plane is a symmetric plane.

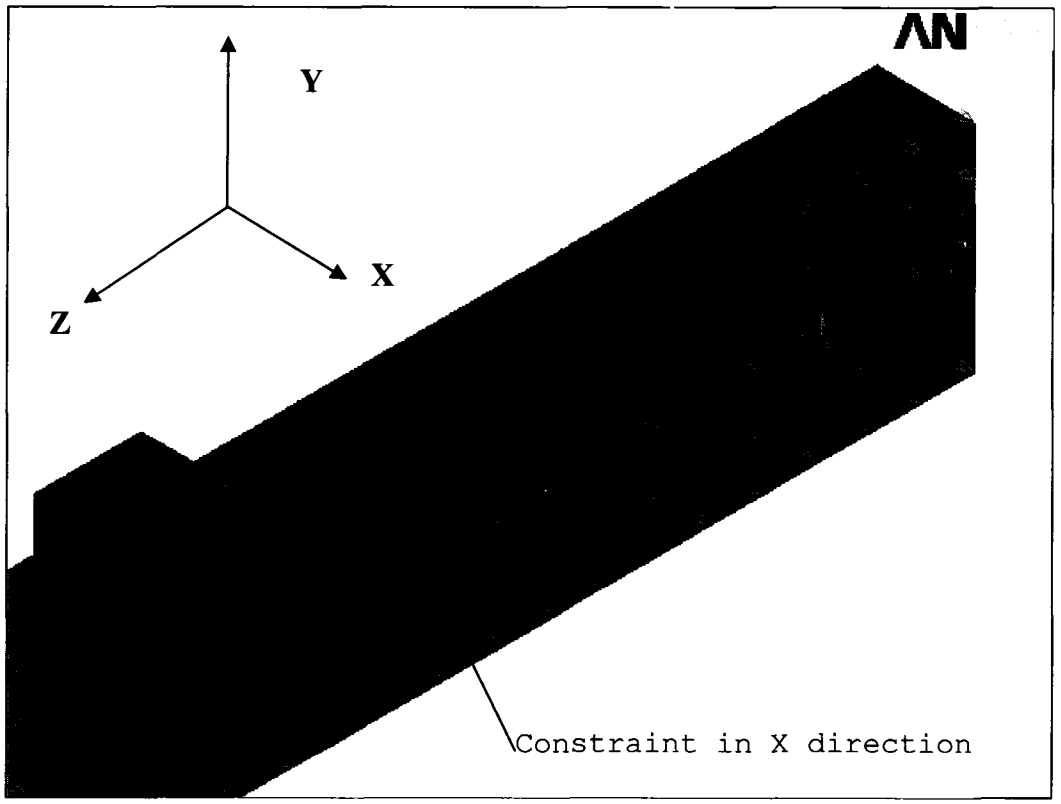

Figure 2.16: Boundary conditions for the plane of symmetry of beam model

The beam has two supports. One support was modeled as a pin end constraint. A single line of nodes on the bottom surface was given constraint of displacement in the X, Y and Z directions. The magnitude of these displacements was set as zero. By doing so, the beam will be allowed to rotate about X-axis. Another support is a roller support. A single line of nodes on the bottom surface was constrained in the X and Y direction, the magnitude of displacement at X and Y direction were set as zero. The support condition is shown in Figure 2.17.

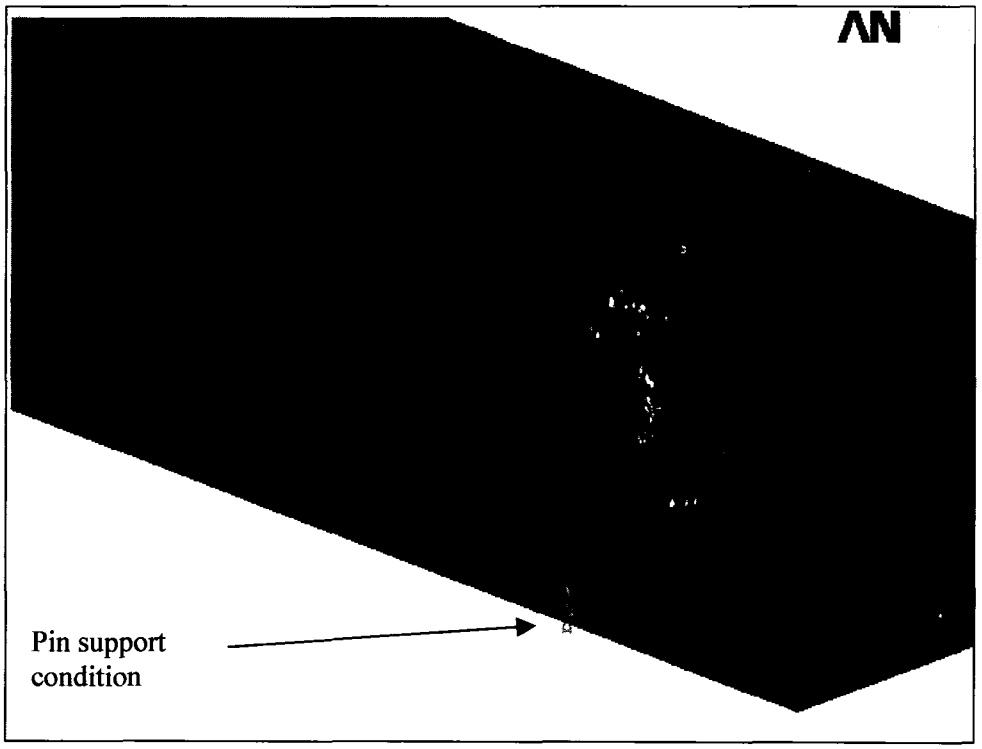

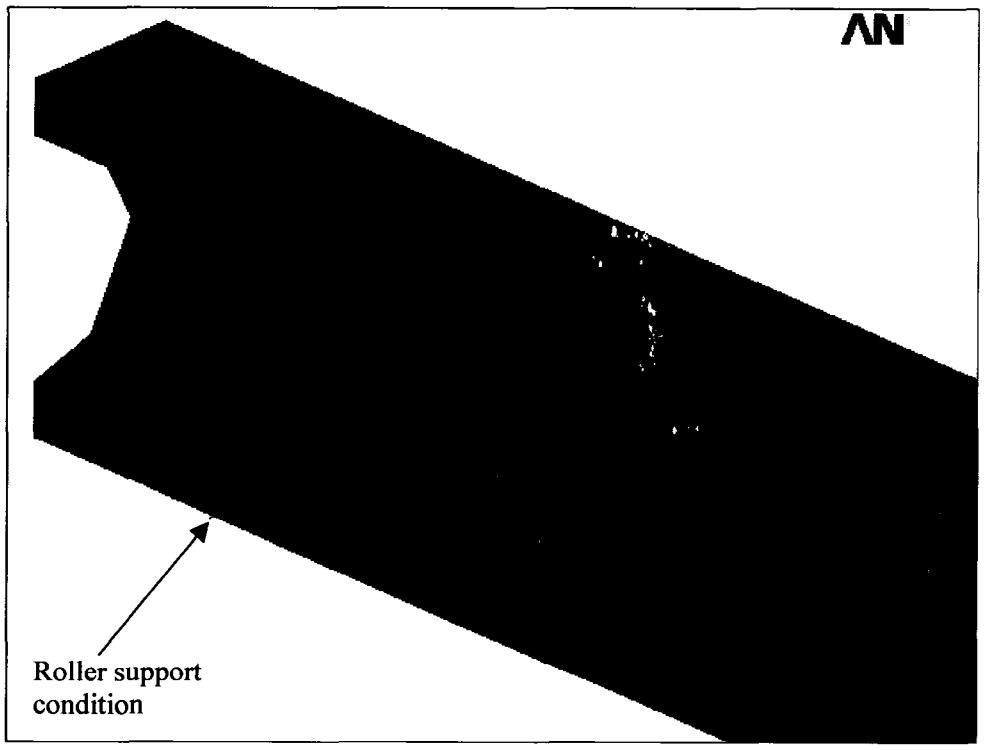

Figure 2.17: Boundary conditions at supports in the beam model

b) Modeling of loading conditions

The concentrated load acting on the steel plate is applied across the centreline of the plate. Because there are 3 nodes along the centreline of the plate, the force applied at each node on the plate is one third of the actual force applied. Figure 2.18 illustrates the simulation of loading condition used in the finite element model.

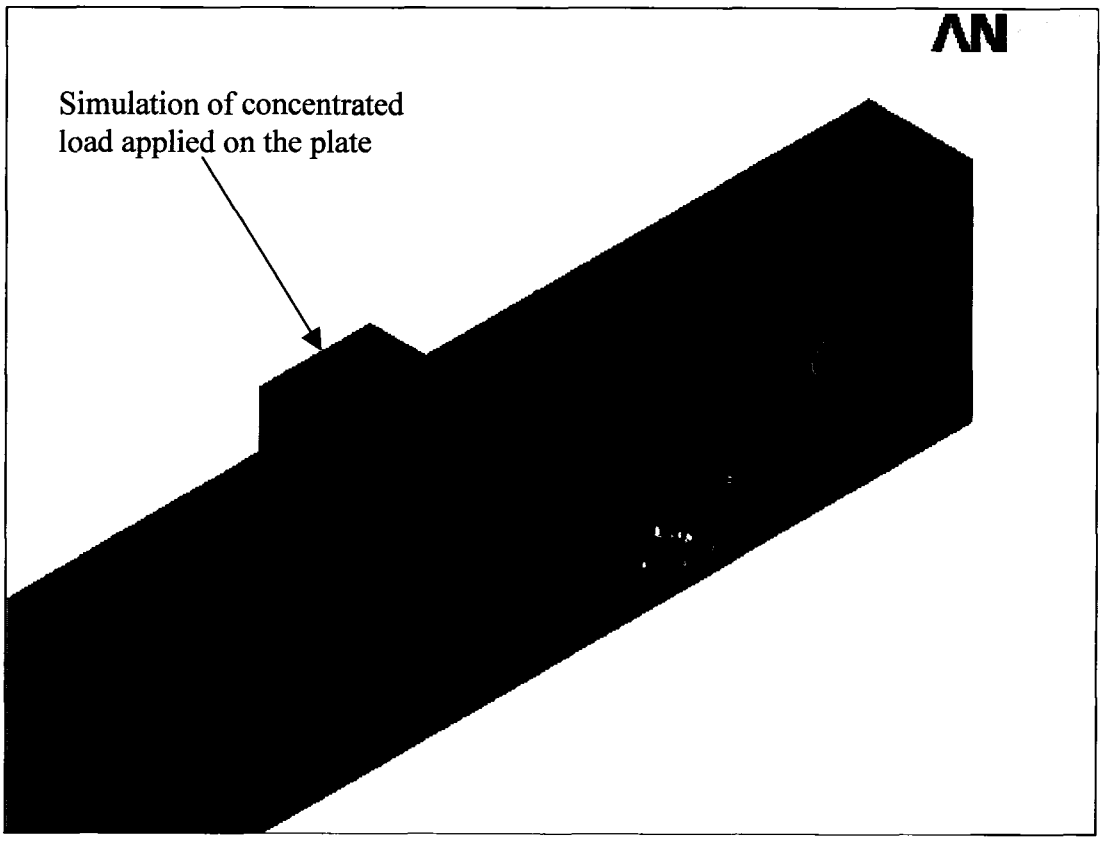

Figure 2.18: Loading condition of the beam model

2.5.2 Hollow core slabs

The slab model is also symmetric about the Z plane, so the nodes on this plane have a displacement constraint along X-axis as zero. Figure 2.19 shows the boundary conditions when Z plane is a symmetric plane.

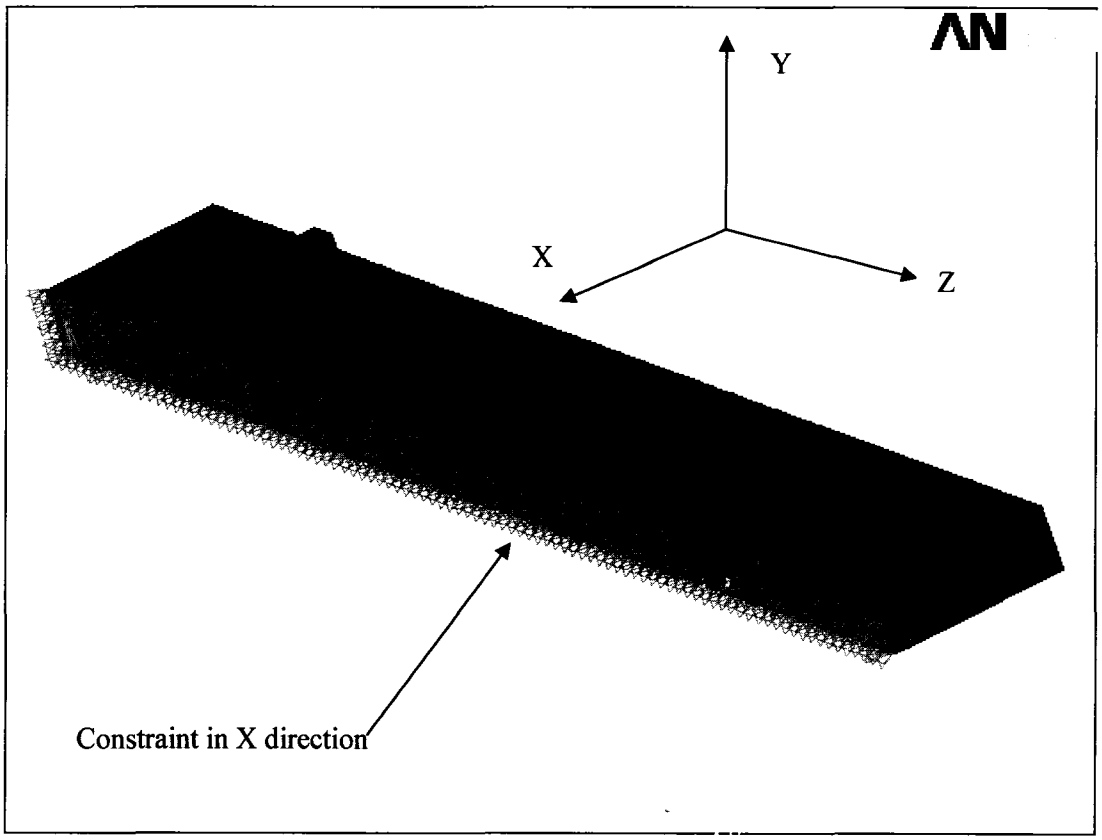

Figure 2.19: Boundary conditions for the plane of symmetry of slab model

The slab has supports at both ends. One of the supports is modeled as a pin end constraint and another support is a roller support. The support condition is shown in Figure 2.20.

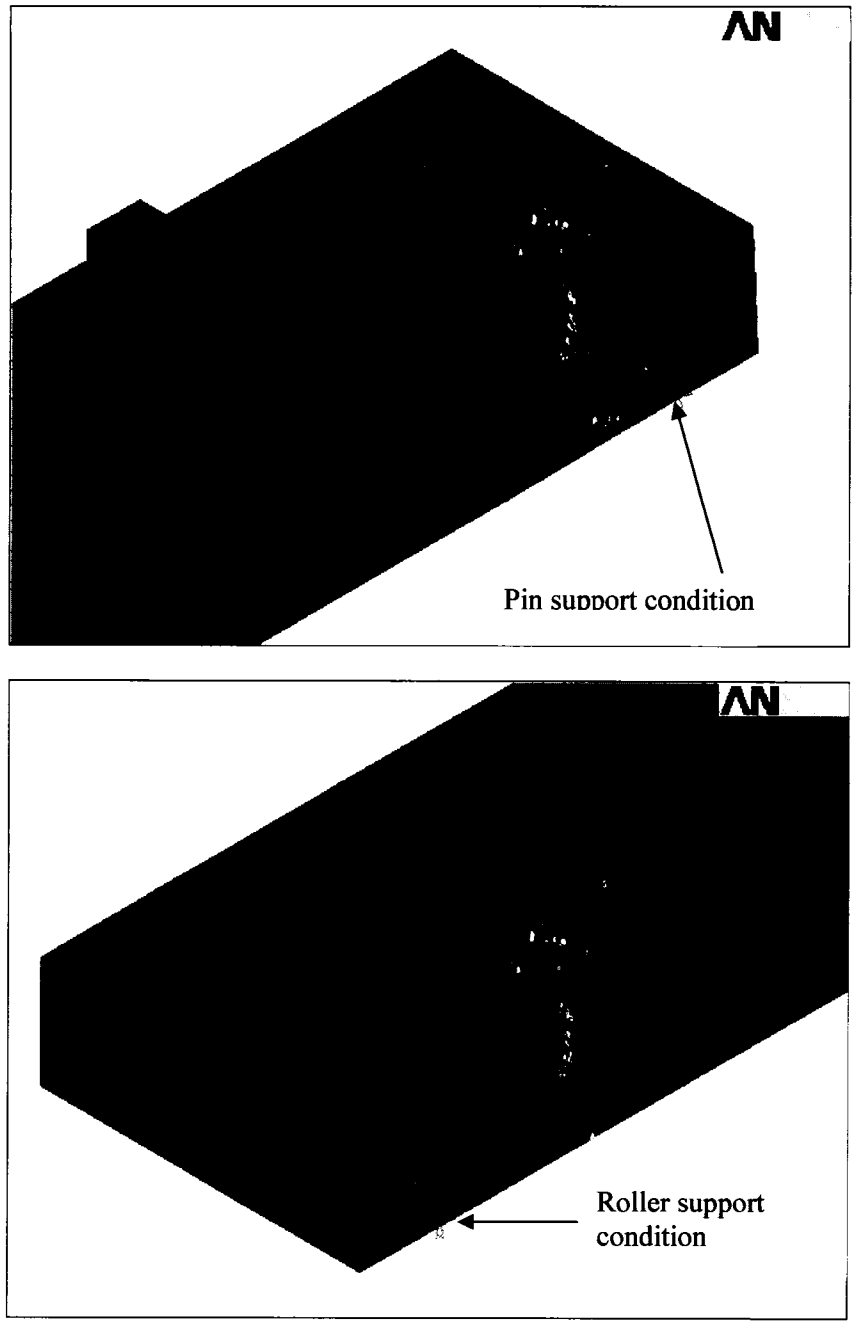

Figure 2.20: Boundary conditions at supports in the slab model

The concentrated load acting on the steel plate is applied across the centreline of the plate.

Figure 2.21 illustrates the simulation of loading condition used in the slab model.

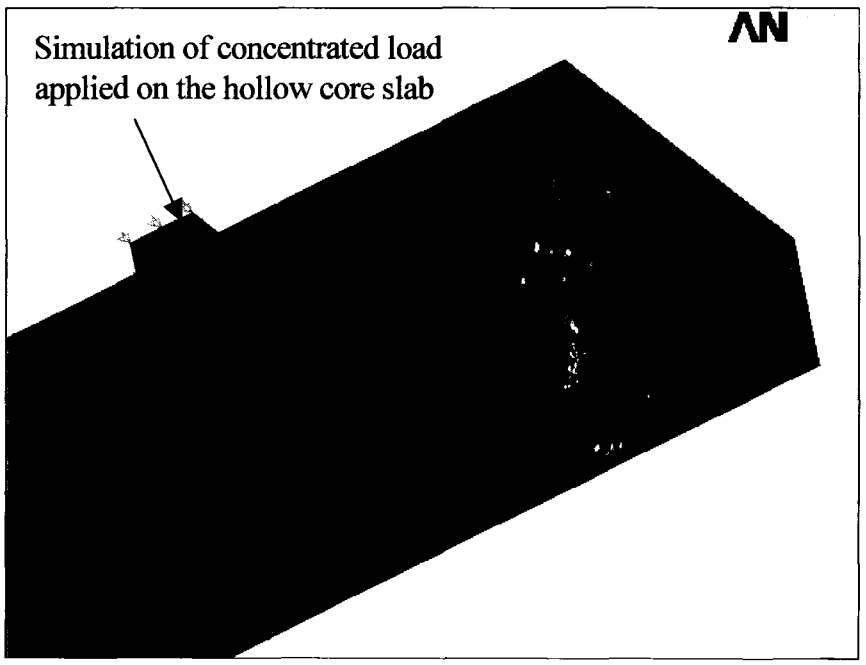

Figure 2.21: Loading condition of the slab model

2.6 Nonlinear Solution for Both Beam and Slab Models

In the nonlinear analysis, the total load applied to a finite element model is divided into a series of load increments called load steps. At the completion of each incremental solution, the stiffness matrix of the model is adjusted to reflect nonlinear changes in structural stiffness before proceeding to the next load increment. The ANSYS program [12] uses Newton-Raphson equilibrium iteration for updating the model stiffness. Newton-Raphson equilibrium iteration provides convergence at the end of each load increment within tolerance. Figure 2.22 shows the use of the Newton-Raphson approach in the nonlinear analysis of a single degree-of-freedom.

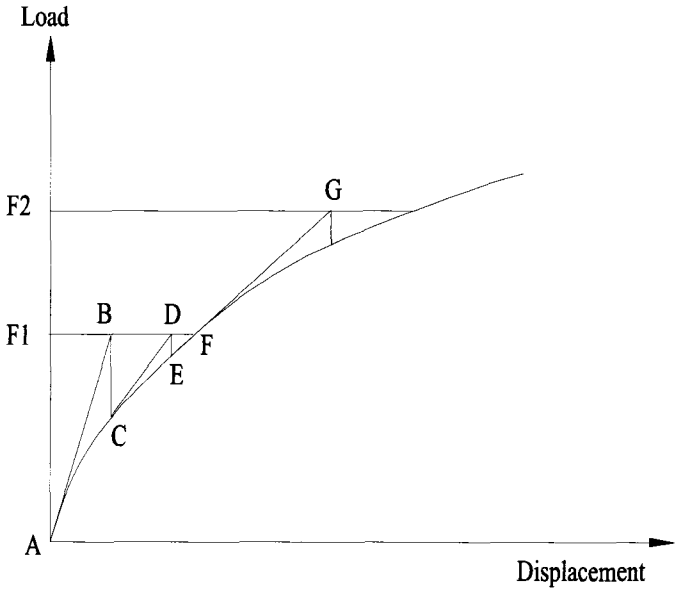

Figure 2.22: Newton-Raphson iterative solution [12]

In the first loading step, the out-of-balance load vector is assessed, which is the difference between the restoring force (the load corresponding to the element stresses) and the applied load. Subsequently, the program carries out a linear solution (from point A to B), using the out-of-balance loads, and checks for convergence. If convergence criterion is not satisfied, the out-of-balance load vector is re-evaluated (back to point C). Then the stiffness matrix is updated (from point C to D), and the convergence is checked again. This iterative procedure continues until the solution converges (reaches point F), so the calculation in the first loading step is completed. The same procedure is then applied to loading steps 2, 3 and so on.

In this study, for the prestressed concrete solid elements, the convergence criteria were based on the force and the displacement. It was found that the convergence of solutions

for the models was difficult to achieve due to the nonlinear behavior of reinforced concrete material. Therefore, the convergence tolerance limits were increased to a maximum of 5 times the default tolerance limits (0.5% for force checking and 5% for displacement checking) in order to obtain convergence of the solutions.

2.7 Load Stepping and Failure Definition for Finite Element Models

The finite element model used in the current analysis is a simple beam under a transverse load. Because there is no live load involved, the "Static analysis type" in ANSYS 2003 is chosen. The "Restart" command is utilized to restart an analysis after the initial run or when the loading step has been completed.

For nonlinear analysis, the "Automatic Time Stepping" function in the ANSYS program will predict and control the size of the load step. Based on the time-history of the previous solution and the physics of the models, if the convergent behaviour is smooth, the "Automatic Time Stepping" function will increase the load increment up to the selected maximum size of load step. If the convergent behaviour is abrupt, the "Automatic Time Stepping" function will bisect the load increment until it is equal to a selected minimum size of load step. The maximum and minimum load step sizes are the required input for utilizing the "Automatic Time Stepping" function in ANSYS.

Failure of the models is defined when the solution for a 1 lb (0.45 kg) load increment does not converge. The program then gives a message specifying that the models have a

significantly large deflection, which exceeds the displacement limitation of the ANSYS program.

CHAPTER 3 Results and Discussions

The purpose of the comparison between the results obtained from finite element analysis and the physical tests of beams and slabs is to ensure that the material properties, real constants and convergence criteria used in the numerical simulation are correct and the developed finite element model is capable to accurately simulate the structural behaviour of the studied beams and slabs.

3.1 Physical Tests

1) Beam-1 (the ratio of the shear span *a* to depth *d*: 3.0)

Figure 3.1 shows the testing set up of Beam-1, which has a shear span length of 23.6 in. (600 mm).

Figure 3.1: Physical set up of Beam-1

The location of load cell and dial indicator on beam-1 is given in Figure 3.2.

This beam was loaded to failure. The computer connected to the dial indicator on the beam recorded the mid-span deflection and the loading history. The load increment is very small (about 0.225 kips or 1.0 kN per 5 second) to ensure the accuracy of the recorded data.

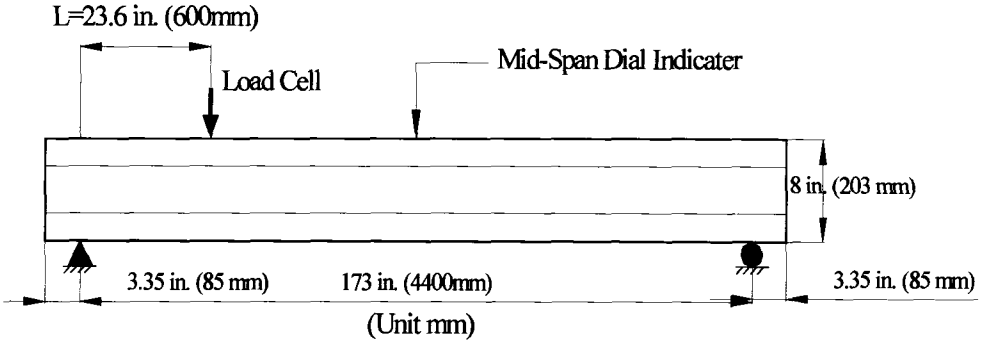

Figure 3.2: Elevation of Beam-1

Beam-1 failed suddenly when the first inclined crack appeared and the load reached 8.76 kips (39.0 kN). It was a typical shear failure because the failure was sudden and brittle. Figure 3.3 shows Beam-1 at failure.

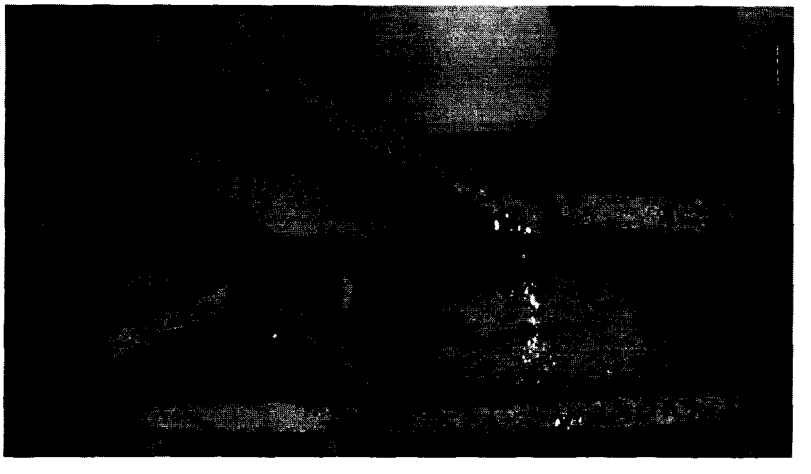

Figure 3.3: Beam-1 at failure

The location of the first crack was on a line drawn from the centreline of the support at an angle of about 40 degrees to the longitudinal axis of the beam. At the time of failure the concrete crushed while the prestressed steel strands did not fail at all.

2) Beam-2 (the ratio of the shear span *a* to depth *d*: 4.25)

Figure 3.4 shows the location of load cell, strain gauge and dial indicator on Beam-2, the shear span length of Beam-2 is 33.5 in. (850 mm).

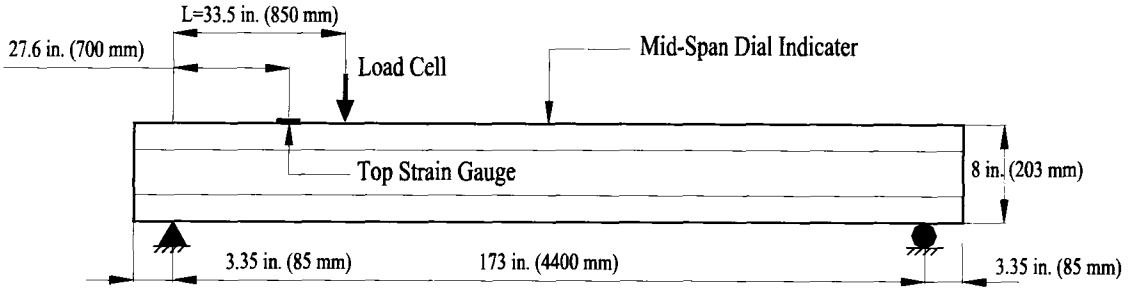

Figure 3.4: Elevation of Beam-2

The first crack occurred at the bottom of the beam when the load reached 5.8 kips (26.0 kN). It then propagated up vertically to the web. When the load increased to 6.9 kips (30.7 kN), the inclined web crack (40 degrees with horizontal plane) occurred and the beam failed. This was still a shear failure. Figure 3.5 (a) shows the first crack on the bottom of beam; Figure 3.5 (b) shows the vertical crack on the web of beam; and Figure 3.5 (c) shows the inclined crack on the web of beam.

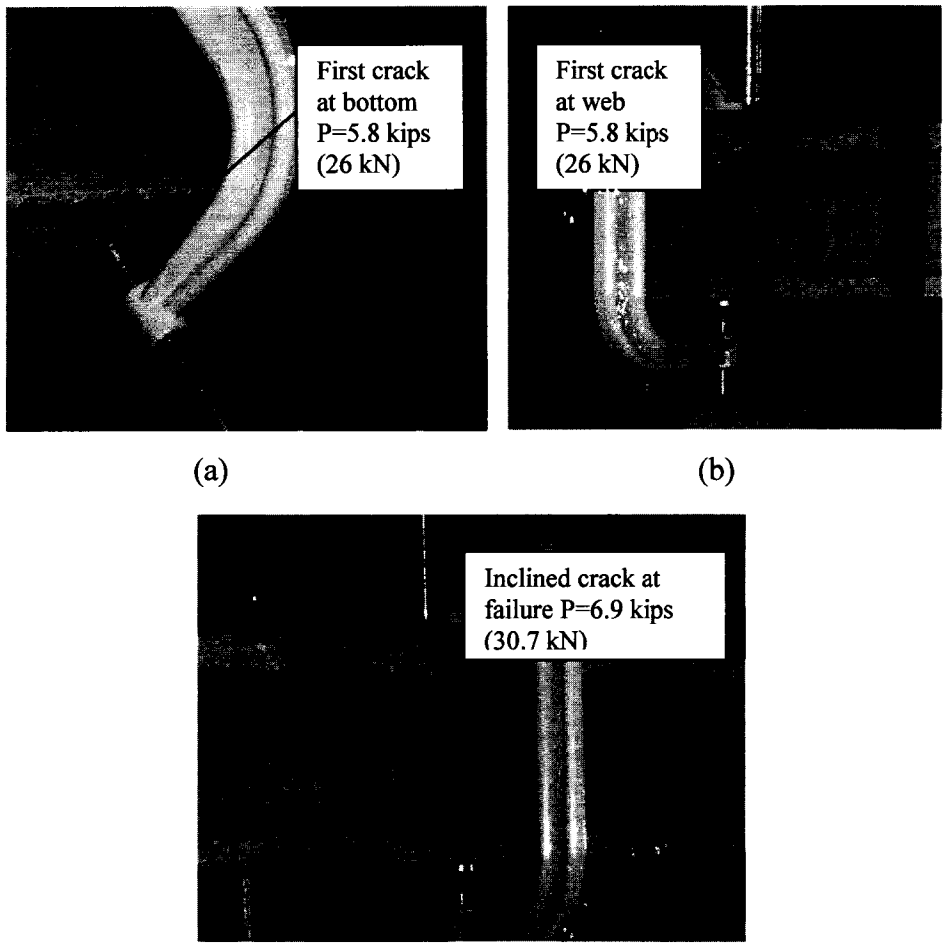

Figure 3.5: Picture of crack on Beam-2

3) Beam-3 (the ratio of the shear span *a* to depth *d*: 3.5)

Beam-3 failed when the load reached 7.2 kips (32.0 kN) and the first inclined crack appeared. The crack formed a 45 degree angle with the longitudinal axis of the beam. It was a typical shear failure because the failure was sudden and brittle. Beam-3 failed in the beginning of the plastic range of the material property. One of the possible reasons could be the imperfection of the concrete material. Figure 3.6 shows Beam-3 at failure.

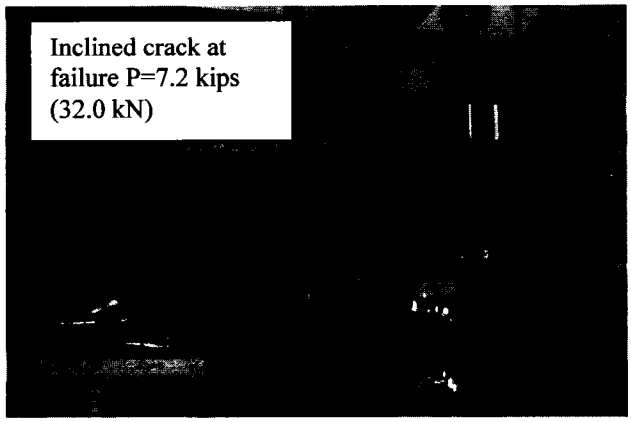

Figure 3.6: Picture of crack on Beam-3

4) Beam-4 (the ratio of the shear span *a* to depth *d*: 2.5)

This beam failed suddenly when the load reached 7.4 kips (33.0 kN) and the first inclined crack appeared. The failure happened within the elastic range of concrete and did not extend to the plastic range. One of the possible reasons could be that this beam is different from the other beams: it has some holes on the top flange, so the beam is already damaged before testing. Figure 3.7 shows Beam-4 at failure.

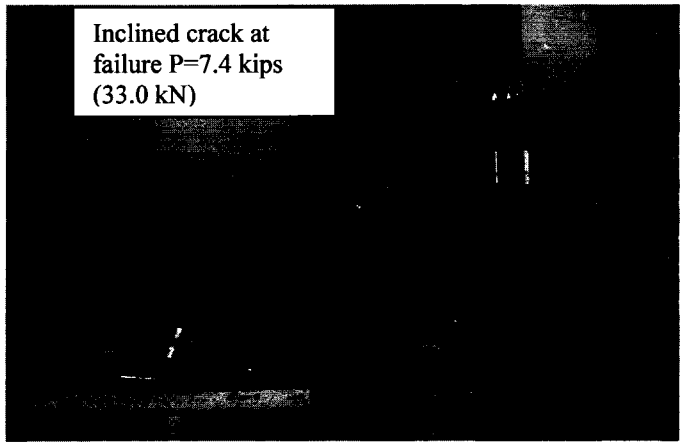

Figure 3.7: Picture of crack on Beam-4

5) Slab-1 (the ratio of the shear span a to depth d: 3.0)

The slabs were tested following the same procedure as the beams. For safety reasons, the slabs were not loaded to their ultimate stage. The loading process was stopped when the width of crack in concrete reached 2 mm.

The first crack on Slab-1 appeared when the load reached 43.8 kips (195.0 kN). It located at the bottom and on the web of the slab. The crack was perpendicular to the longitudinal axis of the slab. The second crack occurred when the load reached 44.3 kips (197 kN). It formed an angle of 70 degree with respect to the longitudinal axis of the slab. The loading process had to be stopped because the width of the first crack was measured to be 2 mm when the load reached 45.2 kips (201 kN). Figure 3.8 (a) shows the first crack, and Figure 3.8 (b) shows the second one.

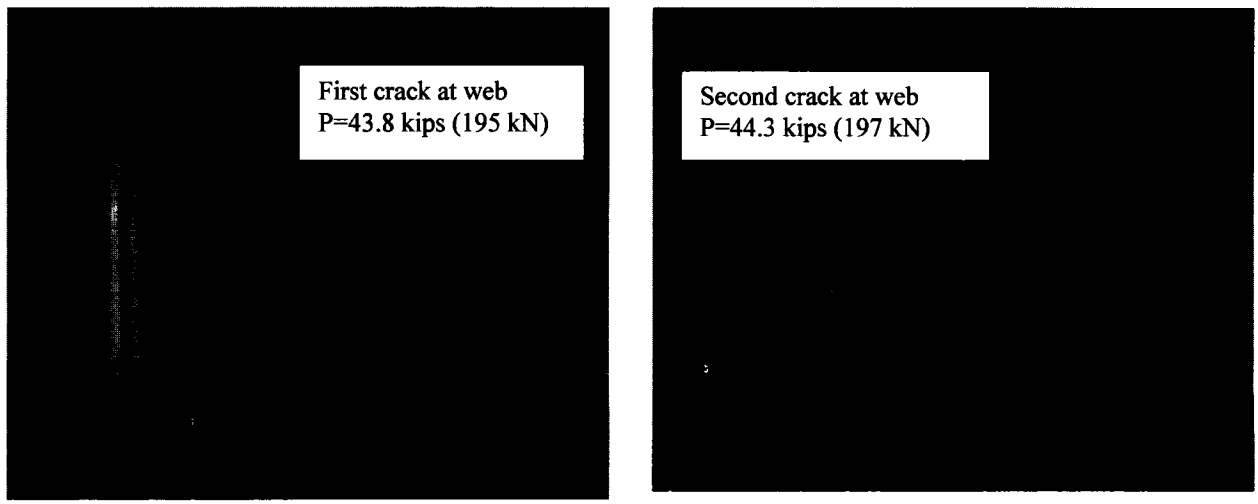

(a) (b)

Figure 3.8: Cracks on Slab-1

6) Slab-2 (the ratio of the shear span *a* to depth *d*: 4.25)

The first crack on Slab-2 was observed when the load reached 33.5 kips (149 kN). It located at both the bottom and the web of the slab and it was perpendicular to the longitudinal axis of Slab-2. The vertical crack on the web went up towards the top of the slab. As the load increased, the crack became more and more inclined when passed 2/3 height of the slab. It formed an angle of 45 degree with respect to the longitudinal axis of the slab. The testing was stopped when the load reached 34.8 kips (155 kN) because the width of bottom crack was measured to be 2 mm. Figure 3.9 (a) shows the first crack on Slab-2 and Figure 3.9 (b) shows the extension of the first crack.

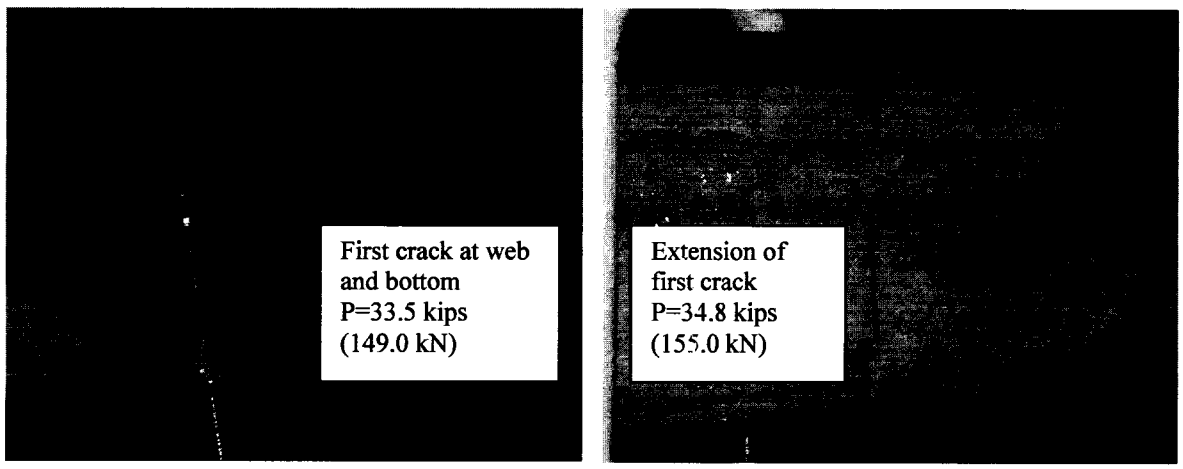

Figure 3.9: Cracks on Slab-2

7) Slab-3 (the ratio of the shear span *a* to depth *d*: 3.5)

The first crack on Slab-3 appeared when the load reached 29.2 kips (130.0 kN). It located at the bottom and the web of the slab. The crack was perpendicular to the longitudinal axis of the slab. The second crack occurred when the load reached 31.5 kips (140.0 kN). It formed an angle of 60 degrees with respect to the longitudinal axis of the slab. The loading process had to be stopped because the width of the first crack was measured to be 2 mm when the load reached 32.6 kips (145.0 kN). Figure 3.10 shows the cracks on Slab-3.

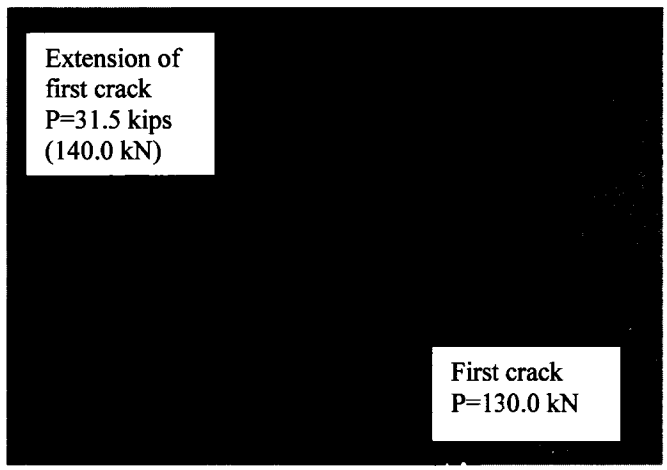

Figure 3.10: Cracks on Slab-3

8) Slab-4 (the ratio of the shear span *a* to depth *d*: 2.5)

The first crack on Slab-4 appeared when the load reached 44.7 kips (199.0 kN). It located at the bottom and the web of the slab. The web crack propagated to the upper part of the web as the load increased. The loading process had to be stopped because the width of

the bottom crack was measured to be 2 mm when the load reached 48.3 kips (215 kN). Figure 3.11 shows the cracks on Slab-4.

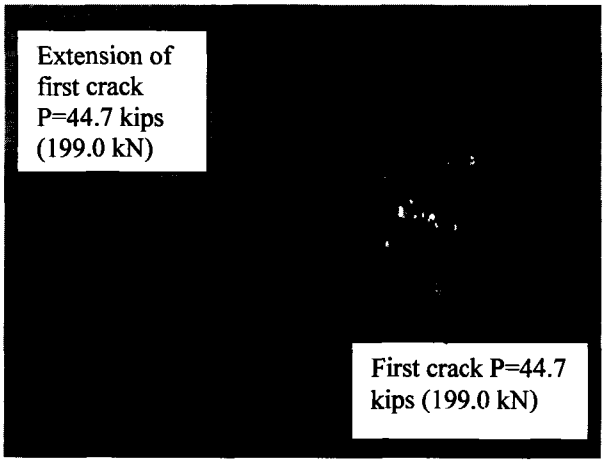

Figure 3.11: Cracks on Slab-4

3.2 Finite Element Analysis

The ANSYS elements, material properties and boundary conditions as previously discussed in section 2.2 were used in the following finite element model. In the finite element model, the application of the load up to failure was done incrementally as required by the Newton-Raphson procedure. After each load increment was applied, the restart option was used to go to the next step after convergence.

The first load step taken was to produce the camber in the concrete beam due to the prestress. The second load step was the addition of the self-weight. After the first 2 loading steps, the time at the end of each step (or sub-step) corresponds to the vertical

loading applied to the beam. For the third load step the time at the end of the load step (or sub-step) is referring to a load applied at the steel plate.

3.3 Comparison of Experimental and Numerical Results

3.3.1 Beams

1) Beam-1

The load-deflection relationship of Beam-1 obtained from the physical experiment and numerical simulation are plotted in Figure 3.12. In the linear part (from point O to point A in Figure 3.12) the numerical results agree very well with the experimental data. This indicates that the modulus of elasticity of concrete used in the numerical model was selected correctly. Moreover, the prestressing effect of steel strands was also properly simulated in the model. In the nonlinear part of the curve (from point A to point B or C), the slope of the experimental curve is steeper than that by finite element analysis. One possible reason could be that the parameter of shear transfer coefficient or the stress-strain curve of concrete in the numerical model is not exactly the same as those in the physical specimen. It can be seen that the maximum service load of 7.0 kips (31.0 kN) predicted by the numerical model agrees well with the physical testing data of 7.2 kips (31.9 kN). It captures well the nonlinear load-deflection response of the beam up to failure. The maximum service load is defined as follows: on the load-deflection curve of a specimen (for example, Beam-1 in Figure 3.12), a point (point A) can be identified

beyond which the displacement increased rapidly with very little increase in load. The load corresponding to this specific point is defined as the maximum service load.

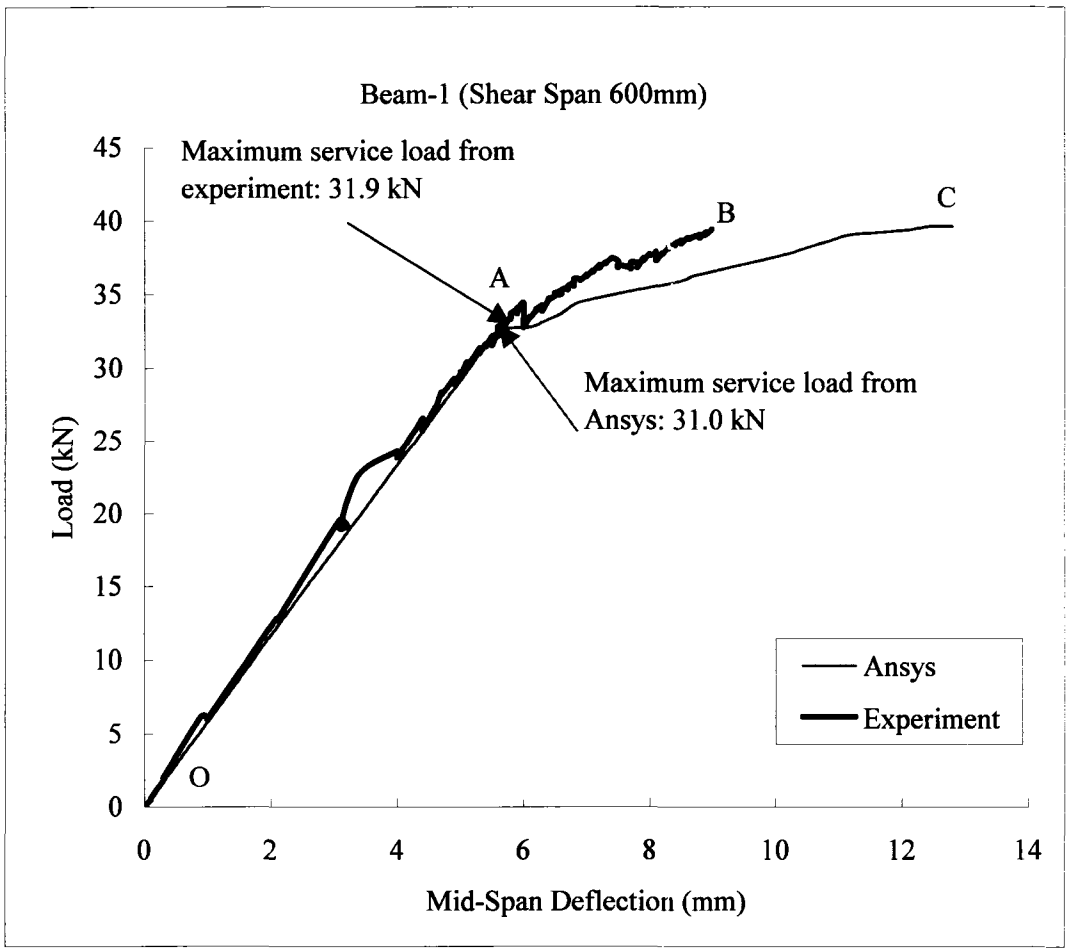

Figure 3.12: Experimental and Numerical load-deflection responses of Beam-1

2) Beam-2

Figure 3.13 shows the load-deflection relationship of Beam-2 obtained from the physical experiment and finite element simulation. The two curves agreed very well in both the linear part and nonlinear part. It means that all the parameters selected for the numerical

model correctly represent the physical properties of Beam-2. In Figure 3.13, it can be seen that the numerical model predicts the maximum service load to be 5.1 kips (22.90 kN) whereas that obtained during the tests was 5.4 kips (24.0 kN). The difference is only 4.6%.

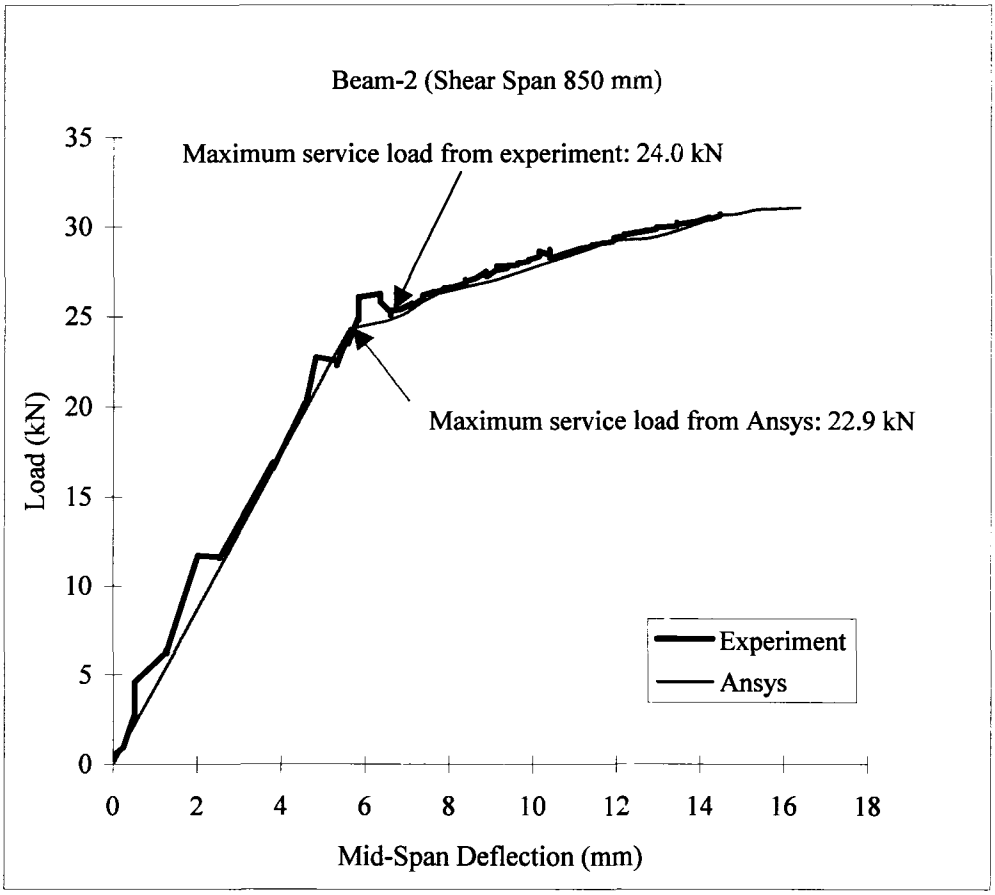

Figure 3.13: Experimental and Numerical load-deflection responses of Beam-2

In the numerical simulation, the first crack(s) of Beam-2 appeared when the load reached 6.2 kips [27.6 kN], while that observed in the experimental work corresponds to a load of 5.8 kips [26.0 kN]. The difference is 5.8%. Figure 3.14 shows the first crack(s) of Beam-

2 in the numerical model. Compared with Figure 3.5 (Pictures of crack on Beam-2), appreciable agreement of crack pattern can be seen from these figures. Both first cracks are perpendicular to the longitudinal axis of the beam and of flexural type. They all occurred at the cross section where the concentrated load is applied, initiated from the bottom flange and extended to the web.

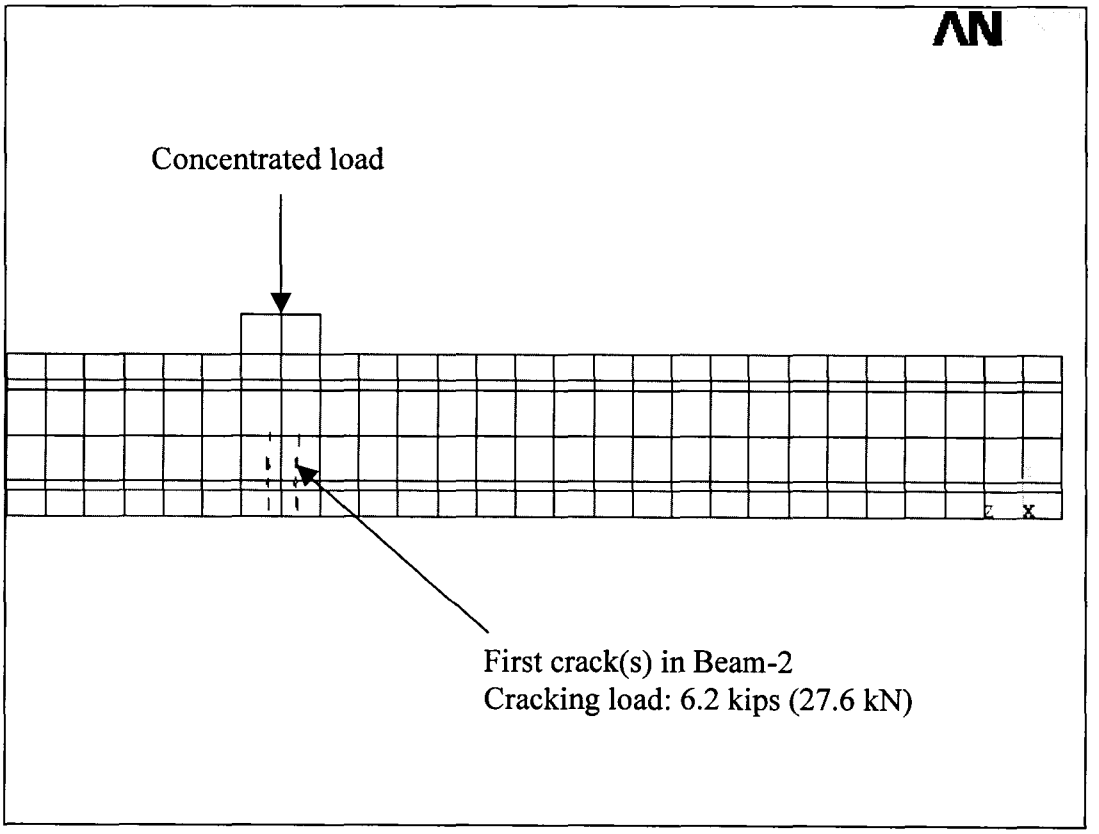

Figure 3.14: First crack(s) of Beam-2 in numerical model

The strain of concrete at the top surface of the beam measured during the tests was compared to the numerical results in Figure 3.15. Again, it was found that the two sets of data agreed very well till the applied load reached approximately 5.6 kips (25.0 kN).

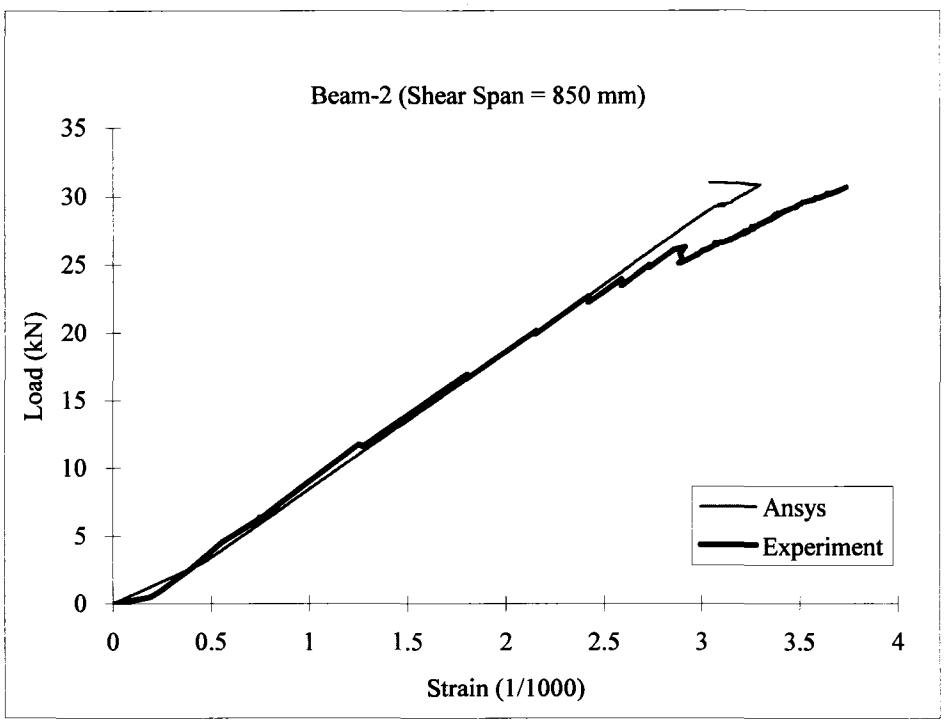

Figure 3.15: Experimental and Numerical load-strain responses of Beam-2

3) Beam-3

The load-deflection relationship of Beam-3 obtained from the physical experiment and numerical simulation is plotted in Figure 3.16. In the elastic range, these two curves agreed reasonably well; but the physical beam failed at the beginning of plastic range while the numerical one went much further in the plastic range. The most possible reason could be that the material properties of concrete have some defects in the mixing and / or

manufacturing process. The maximum service load of 6.1 kips (27.0 kN) observed in the physical test agrees well with the numerical model data of 6.0 kips (26.5 kN).

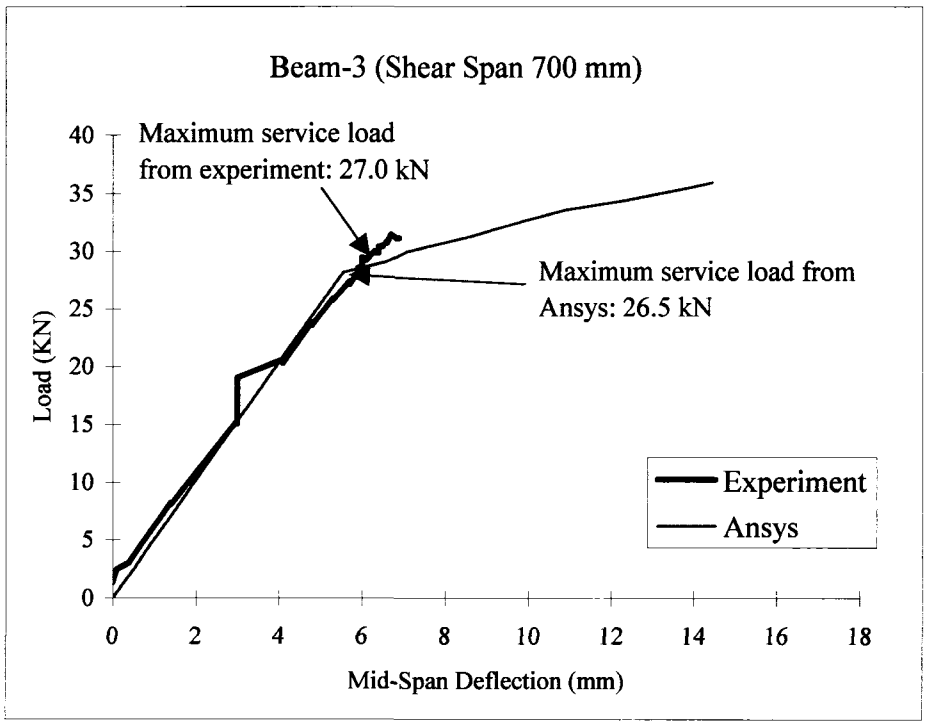

Figure 3.16: Experimental and Numerical load-deflection responses of Beam-3

4) Beam-4

Figure 3.17 shows the load-deflection relationship of Beam-4 obtained from the physical experiment and numerical simulation. It can be seen from Figure 3.17 that the physical beam failed abruptly in the elastic range and did not extend to the plastic range at all. As we discussed in section 3.1, one of the most possible reasons could be that this beam was damaged before testing because it has some holes on the top flange. The maximum

service load of 6.7 kips (30.0 kN) observed in the physical test is much lower than the numerical model data of 8.0 kips (35.5 kN).

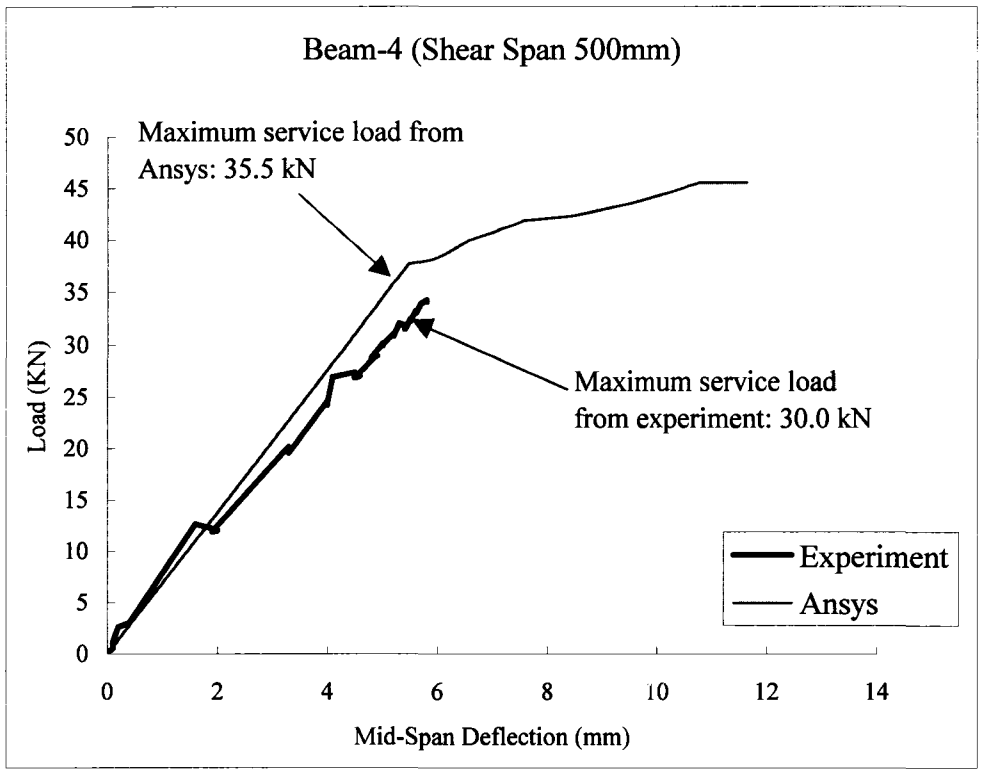

Figure 3.17: Experimental and Numerical load-deflection responses of Beam-4

3.3.2 Slabs

1) Slab-1

The load-deflection relationship of Slab-1 obtained from the physical experiment and the numerical simulation are plotted in Figure 3.18. The two curves agreed reasonably well except that the slope of the numerical curve is steeper than that of the experimental curve. One possible reason could be that the modulus of elasticity of concrete used in the

numerical model (which is taken from the standard test of PSI) is a little bit higher than it should be in the specimen. It can be seen that the maximum service load of 44.6 kips (198.5 kN) predicted by the numerical model agrees very well with the physical testing data of 44.3 kips (197.0 kN).

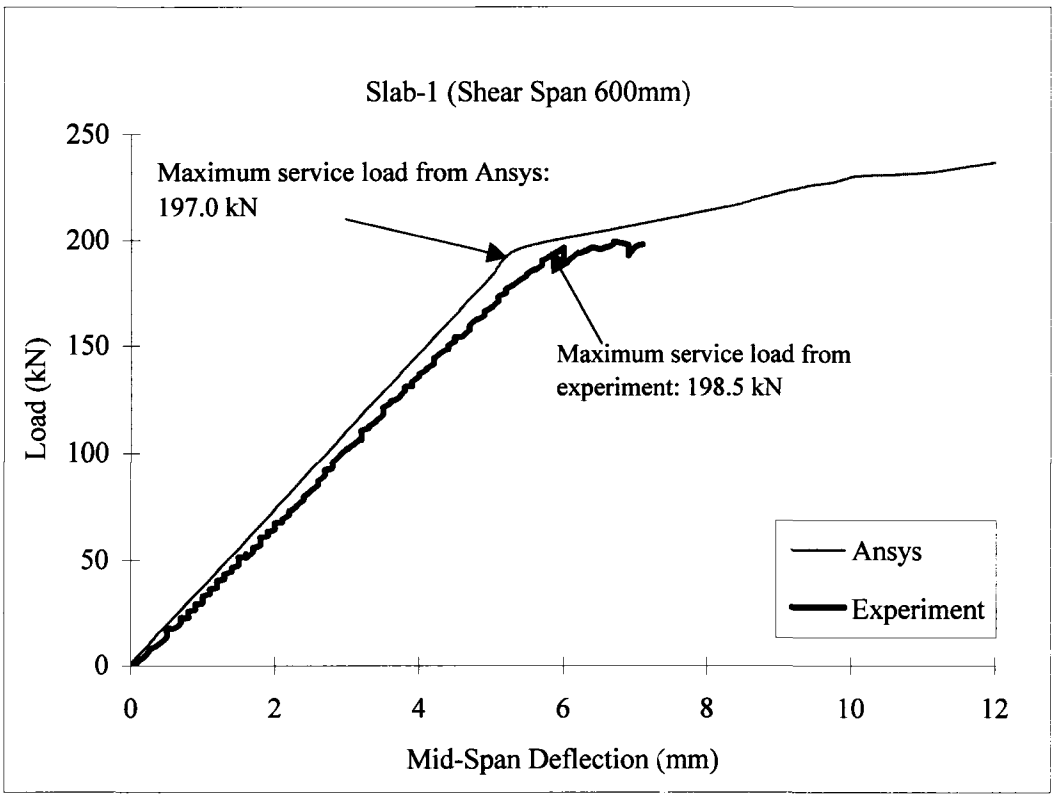

Figure 3.18: Experimental and Numerical load-deflection responses of Slab-1

2) Slab-2

The load-deflection response of Slab-2 is shown in Figure 3.19. In the linear and nonlinear range, the predicted load-deflection response agrees well with the corresponding testing data, except the slope of the curve from the numerical simulation is

slightly steeper than the experimental results. This could be due to that the modulus of elasticity of concrete used in ANSYS model is based on the PSI standard test, which could be slightly different from that of an individual specimen.

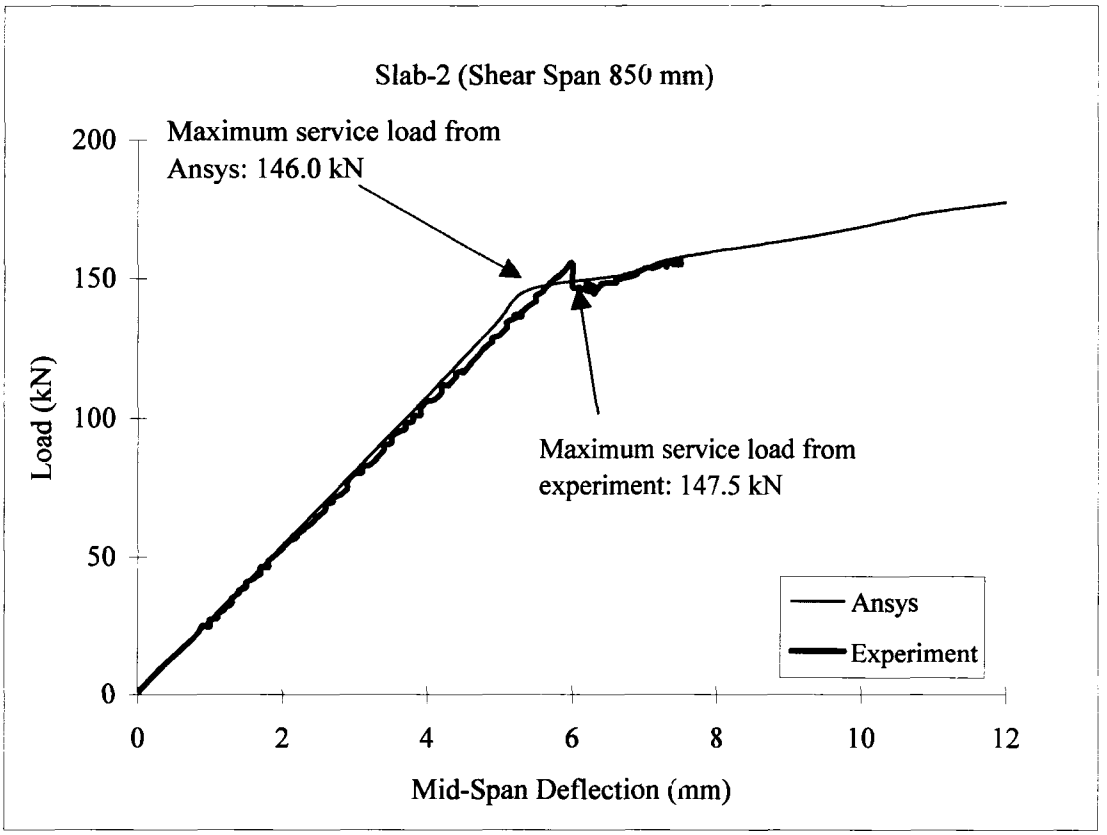

Figure 3.19: Experimental and Numerical load-deflection response of Slab-2

The first cracking load of Slab-2 from the numerical model and the physical test has a difference of 4.2%. The one reported by the numerical model is 34.8 kips [154.9 kN], whereas that observed in the test is 33.5 kips [149.0 kN]. The first crack(s) in the simulation is shown in Figure 3.20. Compared with Figure 3.9 (Cracks on Slab-2), the

crack pattern and the occurred location from the ANSYS simulation are very similar to those from the experiments. Both first cracks are flexural cracks began from the bottom of the slab at the loading location and extended to the web. The maximum service load predicted by the numerical model is 32.8 kips [146.0 kN], and that from the test is 33.1 kips [147.5 kN]. The difference is only 1.0%.

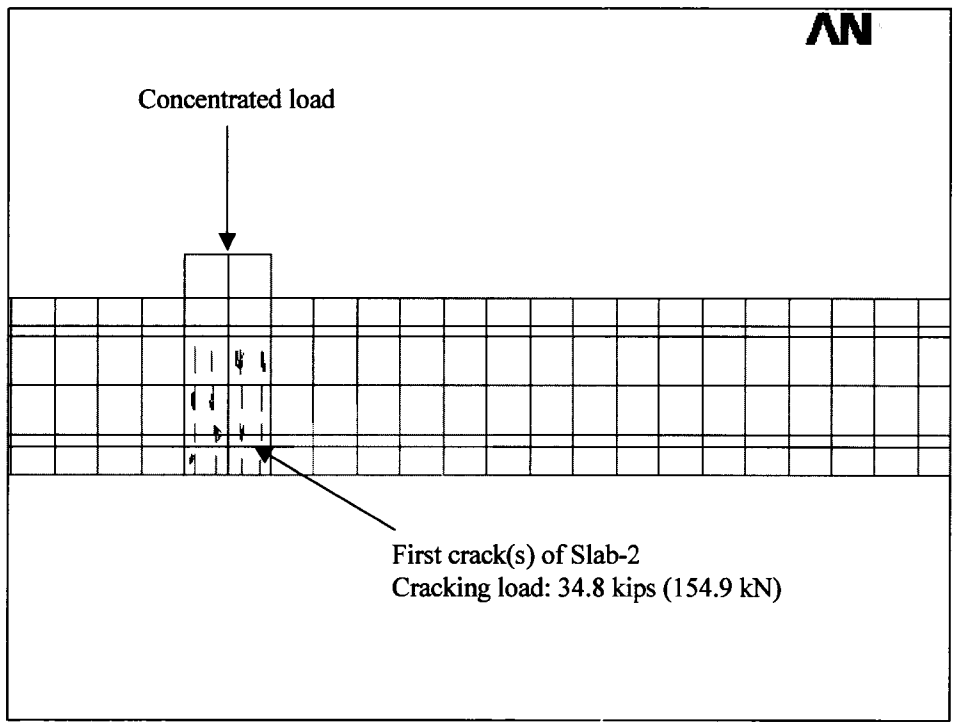

Figure 3.20: First crack(s) of Slab-2 in ANSYS model

3) Slab-3

Figure 3.21 shows the load-deflection relationship of Slab-3 obtained from the physical experiment and the finite element analysis. The maximum service load of Slab-3

predicted by the numerical model was 37.1 kips (165.0 kN) and the maximum service load reached in the tests was 30.3 kips (135.0 kN). The difference is 22.2%. One of the possible reasons that cause this relatively large difference could be that the material properties of concrete have some defects in the mixing and / or manufacturing process.

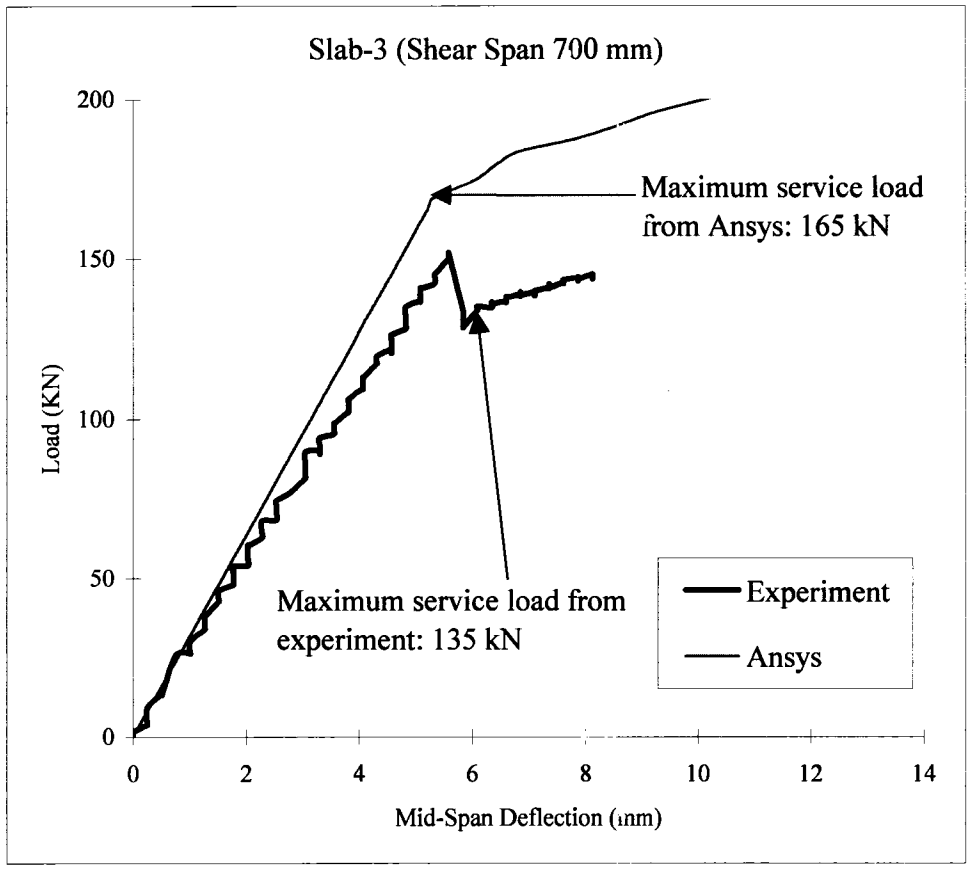

Figure 3.21: Experimental and Numerical load-deflection response of Slab-3

4) Slab-4

The load-deflection relationship of Slab-4 obtained from the physical experiment and the finite element analysis is shown in Figure 3.22. The maximum service load of 47.2 kips

(210.0 kN) predicted by the numerical model and of 43.8 kips (195.0 kN) from the physical test has a difference of 7.7%.

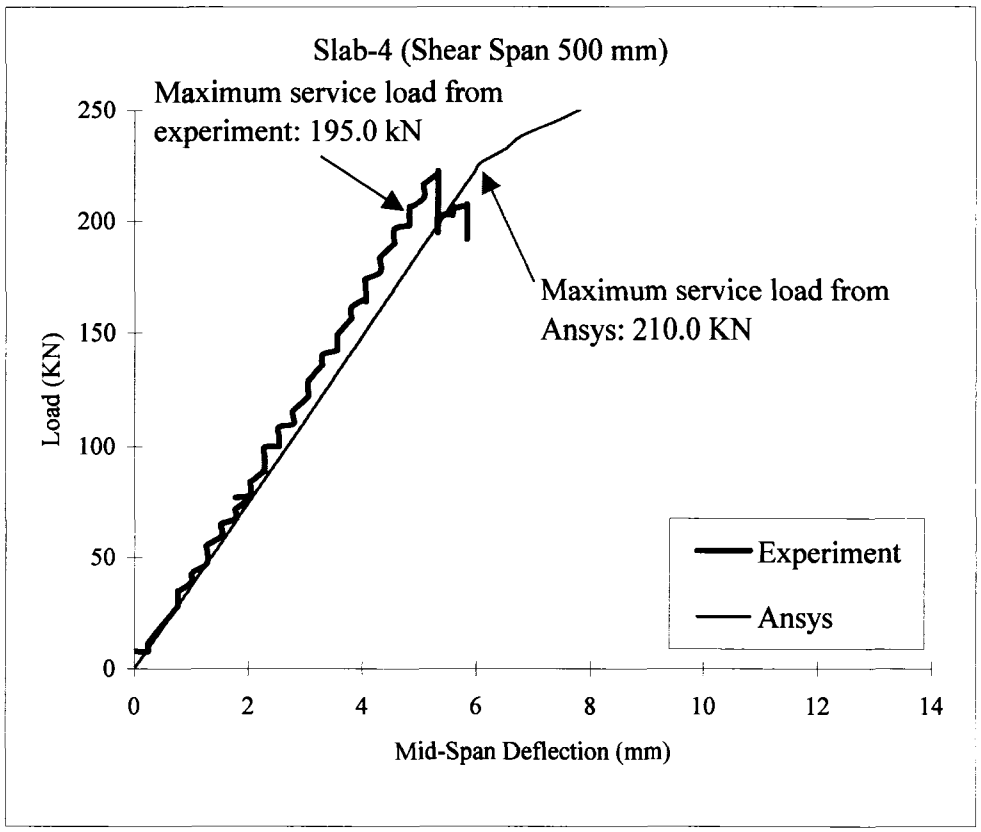

Figure 3.22: Experimental and Numerical load-deflection response of Slab-4

3.4 Comparison with ACI 318 code prediction

The maximum service load obtained from the physical tests and the numerical simulation is applied by a strength-reduction factor to achieve the factored maximum service load. The strength-reduction factor ϕ is taken as 0.75 [13], provided the load factors are following the recommendations in ACI 318-05 Section 9.2. The comparison of the

factored maximum service load of hollow core slabs and I-shaped beams subjected to concentrated load obtained from the numerical simulation, physical experiments and the prediction from the ACI 318 code are summarized and presented in Table 3.1 and Table 3.2.

Table 3.1: Comparison of I-shaped concrete results

		*Beam-4**	Beam-1	Beam-3	Beam-2
Shear span to depth ratio, a/d		*2.5*	3	3.5	4.3
Factored maximum service load, kips (kN)	Test	*5.6 (24.8)*	5.4 (23.9)	4.6 (20.3)	4.0 (17.6)
	ANSYS	*6.0 (26.6)*	5.2 (23.3)	4.5 (19.9)	3.9 (17.2)
	ACI 318 Code	*5.3 (23.4)*	5.1 (22.8)	4.3 (19.2)	3.8 (16.7)
Difference, %	Test & ANSYS	*6.7*	2.8	1.9	2.6
	Test & Code	*6.4*	4.9	5.5	5.5
	ANSYS & Code	*13.7*	1.9	3.4	2.8

Table 3.2: Comparison of hollow core slab results

		Slab-4	Slab-1	*Slab-3**	Slab-2
Shear span to depth ratio, a/d		2.5	3.0	*3.5*	4.3
Factored maximum service load, kips (kN)	Test	32.9 (146.3)	33.5 (148.9)	*22.8 (101.3)*	24.9 (110.6)
	ANSYS	35.4 (157.5)	33.2 (147.8)	*27.8 (123.8)*	24.6 (109.5)
	ACI 318 code	28.4 (126.5)	27.6 (122.6)	*23.3 (103.8)*	20.5 (91.3)
Difference, %	Test & ANSYS	7.7	0.8	*18.2*	1.0
	Test & Code	13.5	17.6	*2.4*	17.5
	ANSYS & Code	19.7	17.0	*16.2*	16.6
Reevaluated effective web width $b_{w\ new}$		1.2 b_w	1.2 b_w	1.2 b_w	1.2 b_w

* The data in this column is not used for comparison because this specimen is not working well during physical test.

It can be seen from these two tables that in general, the experimental results are greater than the numerical simulation, and ACI 318 code gives the least prediction. For the factored maximum service load of I-shaped beams given in Table 3.1, the largest

difference among the three sets of results is only 5.5%. Table 3.2 shows the comparison of the factored maximum service load of the hollow core slabs. It can be seen that the numerical predictions agree well with the experimental results, especially in the case of Slab-1 and Slab-2. The average difference between these two sets of results is 0.9%. However, the results obtained from ACI 318 code are much smaller than those from ANSYS simulation and experiments. The average factored maximum service load obtained from ANSYS and test are 17.8 % and 16.2 % higher than the ACI 318 code predictions, respectively. For the code prediction, the factored maximum service load of the I-shaped beam and the hollow core slab is determined based on the less of Eq. (1.1) and (1.2). While the I-shaped beam is considered as a single web hollow core slab, of which the net web width is taken exactly the same as the web width of the beam, in the case of the multi-web hollow core slab, the simple summation of the minimum parts of the slab web as b_w neglects the potential interaction between the adjacent webs. This could underestimate the actual effective web width of the hollow core slab and lead to a more conservative prediction of its shear strength.

If the numerically obtained factored maximum service load is applied to the left side of the equation (Eq. (1.1) or (1.2), depending on the failure mode), a re-evaluated effective web width of hollow core slab b_{w_new} can be obtained. It is also presented in Table 3.2, which is 20% higher than the original b_w.

CHAPTER 4 Conclusions and Recommendations

In the present study, finite element models are developed to study the shear behaviour of I-shaped concrete beams and prestressed concrete hollow core slabs. The results obtained from the numerical simulations are compared with those from the physical tests and ACI 318 code. Based on these comparisons, the following conclusions can be drawn:

1. The finite element models developed in the present study can accurately simulate the shear behaviour of I-shaped concrete beams and prestressed concrete hollow core slabs. The response in terms of the load-deflection relation at the mid-span of the specimens obtained from the ANSYS simulation agrees well with what observed in the tests. The maximum service load and cracking load predicted by the numerical models are very close to the experimental results.
2. The shear capacity predicted by the ACI 318 code agrees well with the ANSYS simulation and the physical test for the I-shaped concrete beams, but it is more conservative in the case of the prestressed hollow core slabs. One possible explanation could be that when determine the effective web width for shear strength calculation of hollow core slabs, the current ACI 318 code ignores the interaction between the adjacent webs, which results in a more conservative prediction.

As future work, more studies are required to quantify the impact of the web interaction on the shear capacity of prestressed concrete hollow core slabs.

APPENDIX A Calculation of shear capacity of I-shaped concrete beams

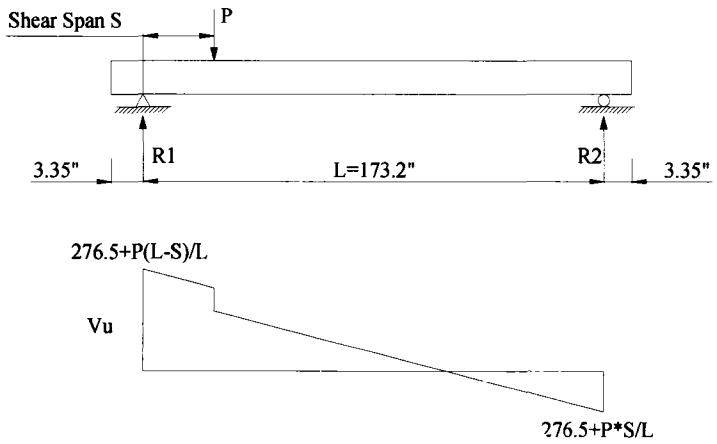

Figure A.1 I-shaped concrete beams with supports

Prestressing Steel: 0.5 *in* diameter, $f_{pu} = 270\ ksi$, low relaxation strands,

Initial stress = 70% f_{pu} ; loss = 15%; $f_c^{'} = 6000\ psi$; L = 173.2 in;

$b_w = 1.89\ in$; $d = 6.8\ in$; $V_p = 0$

$$V_{cw} = (3.5\sqrt{f'_c} + 0.3 f_{pc}) b_w d_p + V_p$$

$$= (3.5\sqrt{6000} + 0.3 f_{pc}) \times 1.89 \times 6.8 + 0$$

$$= 12.85 \times (271.1 + 0.3 f_{pc})$$

$$= 3484 + 3.86 f_{pc}$$

f_{pc} is calculated as a function of the transfer of prestress into the section along the span.

Transfer length = $50\ d_b = 50 \times 0.5 = 25$ "

Bearing length = 3.35 "

Full prestress transfer is achieved $(25 - 3.35) = 21.65\ in$" from the face of support.

$$A_{ps} f_{se} = 0.153 \times 270000 \times 0.7 \times (1 - 0.15) \times \left(\frac{x + 3.35}{25}\right)$$

to $x = 21.65$"

$$A_{beam} = 0.203 \times 0.187 - \frac{1}{4} \times \pi \times 0.139^{2} = 0.0228\ m^{2}$$

$$f_{pc} = \frac{A_{ps} f_{se}}{A} = 682.98 \times \left(\frac{x + 3.35}{25}\right)$$

$$V_{cw} = (4514.13 + 123.92\, x)\, lb \qquad \text{(x from 3.35 to 25 in)}$$

at left support, $V_{cw} = (4514.13 + 123.92 \times 3.35) = 4929.1\, lb$

self weight of HC beam

$$= A_{beam} \times l \times \gamma_{beam} = 0.0228 \times 4.57 \times 2400 = 250\ kg = 551.2\, lb$$

Maximum shear happened at left support, so,

$$P \times \left(\frac{L - S}{L}\right) + \frac{551.2}{2} = 4929.1$$

(1) Shear span S = 500 mm (19.7 in), P = 5249 lb = 23.4 KN

(2) Shear span S = 600 mm (23.6 in), P = 5387 lb = 24.0 KN

(3) Shear span S = 700 mm (27.6 in), P = 5533 lb = 24.6 KN

(4) Shear span S = 850 mm (33.5 in), P = 5766 lb = 25.7 KN

$$\phi V_{ci} = 0.85 \times \left(0.6\sqrt{6000} \times b_{w} d + V_{d} + \frac{V_{i} M_{cr}}{M_{\max}}\right)$$

$$V_{d} = 0.61 \times 56.5 \times (14.44 / 2 - x)$$

$$M_{cr} = (\frac{I}{Y_b})(6 \times \sqrt{6000} + f_{pe} - f_d)$$

$$f_{pe} = A_{ps} f_{se} (\frac{1}{A} + \frac{ey_b}{I})$$

$$A = 35.3 in^2 \qquad A_{ps} = 0.153\ in^2 \qquad I = 269.17\ in^4 \qquad y_b = 4 in$$

$$S = 67.36\ in^4$$

$$f_d = \frac{M_d}{S}$$

$$M_d = 56.5 \times 0.61 \times 14.44 \times 0.5x - 56.5 \times 0.61 \times 0.5x^2$$

$$M_u = R_1 x - 1.4 \times 56.5 \times 0.61 \times 0.5x^2$$

$$M_{max} = M_u - M_d$$

Based on these definitions, ϕV_{ci} are calculated. A summary of ϕV_{cw} and ϕV_{ci} are presented in the following table.

Table A-1 Allowable Shear of I-shaped concrete beams

x	ϕV_{cw}	ϕV_{ci}	Allowable Shear
500 mm (1.64 ft)	23.4 kN	23.4 kN	23.4 kN
600 mm (1.97 ft)	24.0 kN	22.8 kN	22.8 kN
700 mm (2.30 ft)	24.6 kN	19.2 kN	19.2 kN
850 mm (2.79 ft)	25.7 kN	16.7 kN	16.7 kN

APPENDIX B Calculation of shear capacity of hollow core slabs

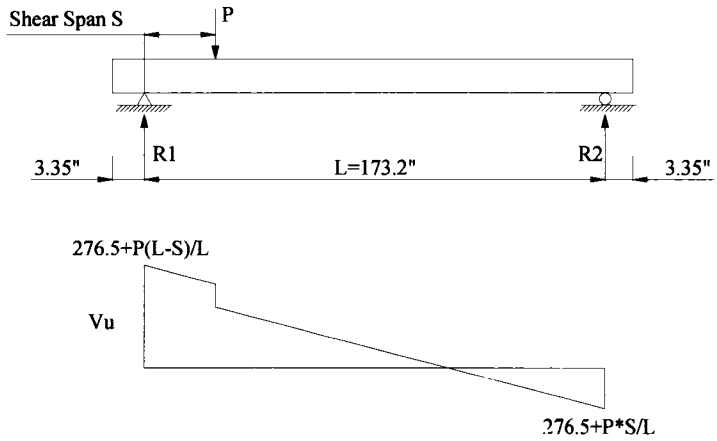

Figure B.1 Prestressed concrete Hollow core slab with supports

Prestressing Steel: 0.5 *in* diameter, $f_{pu} = 270\ ksi$, low relaxation strands,

Initial stress = 70% f_{pu} ; loss = 15%; $f_c^{'} = 6000\ psi$; L = 173.2 in;

$b_w = 13.375\ in$; $d = 6.8\,in$; $V_p = 0$

$$V_{cw} = (3.5\sqrt{f'_c} + 0.3 f_{pc}) b_w d_p + V_p$$

$$= (3.5\sqrt{6000} + 0.3 f_{pc}) \times 13.375 \times 6.8 + 0$$

$$= 90.95 \times (271.1 + 0.3 f_{pc})$$

$$= 24657 + 27.3 f_{pc}$$

f_{pc} is calculated as a function of the transfer of prestress into the section along the span.

Transfer length = $50\, d_b = 50 \times 0.5 = 25$ "

Bearing length = 3.35 "

Full prestress transfer is achieved $(25 - 3.35) = 21.65\ in$" from the face of support.

$$A_{ps} f_{se} = 5 \times 0.153 \times 270000 \times 0.7 \times (1 - 0.15) \times (\frac{x + 3.35}{25})$$

to $x = 21.65$"

$$A_{slab} = 138700\ mm^2 / (25.4)^2 = 215.00\ in^2$$

$$f_{pc} = \frac{A_{ps} f_{se}}{A} = \frac{122897}{215} \times (\frac{x + 3.35}{25})$$

$$V_{cw} = (26748 + 624\ x)lb \qquad \text{(x from 3.35 to 25 in)}$$

at left support, $V_{cw} = (26748 + 624 \times 3.35) = 28838\ lb$

self weight of HC beam

$$= A_{slab} \times l \times \gamma_{beam} = 0.1387 \times 4.57 \times 2400 = 1521\ kg = 3354\ lb$$

Maximum shear happened at left support, so,

$$P \times \left(\frac{L - S}{L}\right) + \frac{3354}{2} = 28838$$

(1) Shear span S = 500 mm (19.7 in), P = 30518 lb = 136.2 KN

(2) Shear span S = 600 mm (23.6 in), P = 31583 lb = 141.0 KN

(3) Shear span S = 700 mm (27.6 in), P = 32333 lb = 144.3 KN

(4) Shear span S = 850 mm (33.5 in), P = 33532 lb = 149.7 KN

$$\phi V_{ci} = 0.85 \times (0.6\sqrt{6000} \times b_w d + V_d + \frac{V_i M_{cr}}{M_{max}})$$

$$V_d = 4 \times 56.5 \times (14.44 / 2 - x)$$

$$M_{cr} = (\frac{I}{Y_b})(6 \times \sqrt{6000} + f_{pe} - f_d)$$

$$f_{pe} = A_{ps} f_{se} (\frac{1}{A} + \frac{ey_b}{I})$$

$$A = 215\ in^2 \qquad A_{ps} = 0.765\ in^2 \qquad I = 1664\ .94\ in^4 \qquad y_b = 4\ in$$

$$S = 415\ in^4$$

$$f_d = \frac{M_d}{S}$$

$$M_d = 56.5 \times 4 \times 14.44 \times 0.5x - 56.5 \times 4 \times 0.5x^2$$

$$M_u = R_1 x - 1.4 \times 56.5 \times 4 \times 0.5x^2$$

$$M_{max} = M_u - M_d$$

Based on these definitions, ϕV_{ci} are calculated. A summary of ϕV_{cw} and ϕV_{ci} are presented in the following table.

Table B-1 Allowable Shear of prestressed hollow core slabs

x	ϕV_{cw}	ϕV_{ci}	Allowable Shear
500 mm (1.64 ft)	136.2 kN	126.5 kN	126.5 kN
600 mm (1.97 ft)	141.0 kN	122.6 kN	122.6 kN
700 mm (2.30 ft)	144.3 kN	103.8 kN	103.8 kN
850 mm (2.79 ft)	149.7 kN	91.3 kN	91.3 kN

REFERENCES

1) Gabrielsson, H. *Prestressed Hollow Core Slabs subjected to Shear, Flexural and Bending*, Luleå University of Technology, Department of Civil and Mining Engineering, Division of Structural Engineering, Luleå, Sweden, 1997.

2) Deuring M *Post-strengthening of Concrete Structures with Pre-stressed Advanced Composites*, Report No. 224, CH-8600, EMPA, Switzerland, 1993

3) Yang, L. *Design of Prestressed Hollow core Slabs with Reference to Web Shear Failure.* Volume 120, pp. 2675-2696. ASCE Journal of structural Engineering, 1994.

4) Matti Pajari, *Resistance of Prestressed Hollow Core Slabs Against Web Shear Failure.*Espoo, VTT Building and Transport, 2005.

5) Faherty, K.F., *An Analysis of a Reinforced and a Prestressed Concrete Beam by Finite Element Method,* Doctorate's Thesis, University of Iowa, Iowa City, 1972.

6) Kachlakev, *Finite element modeling of reinforced concrete structures strengthened with FRP laminates.* Salem, American, 2001.

7) Anthony J. Wolanski, *Flexural Behaviour of Reinforced and Prestressed Concrete Beams Using Finite Element Analysis*, Master Thesis, Faculty of Graduate School, Marquette University, 2004.

8) Buckhouse, E.R., "External Flexural Reinforcement of Existing Reinforced Concrete Beams Using Bolted Steel Channels," Master's Thesis, Marquette University, 1997.

9) Bangash, M. Y. H., Concrete and Concrete Structures: Numerical Modeling and Applications, Elsevier Science Publishers Ltd., London, England, 1989.

10) Willam, K. J., and Warnke, E. D., "*Constitutive Model for the Triaxial Behavior of Concrete",* Proceedings, International Association for Bridge and Structural Engineering, Vol. 19, ISMES, Bergamo, Italy, 1975.

11) Kupfer H B, Hilsdorf H K, Rusch H. *Behavior of Concrete under Biaxial Stresses.* ACI Journal, 1969.

12) ANSYS, *ANSYS User's Manual Revision 2003*, ANSYS, Inc., Canonsburg, Pennsylvania, 2003.

13) ACI 318 – 05, American Concrete Institute, *Building Code Requirements for Structural Concrete and Commentary,* ACI committee, American, 2005.

14) Bathe, K. J., Finite Element Procedures, Prentice-Hall, Inc., Upper Saddle River, New Jersey, 1996.

15) Adams, V. and Askenazi, A., Building Better Products with Finite Element Analysis, OnWord Press, Santa Fe, New Mexico, 1998.

VITA AUCTORIS

NAME:	Xuefei Wang
PLACE OF BIRTH:	Liaoning, China
YEAR OF BIRTH:	1974
EDUCATION:	Northern Jiaotong University, Beijing, China
	1992-1996 B. Sc.
	University of Windsor, Windsor, Ontario
	2005-2007 M.A.Sc.